Accepted Manuscript

The origin of nelsonite and high-Zr ferrodiorite associated with Proterozoic anorthosite

Jean-Clair Duchesne, Jean-Paul Liégeois

PII: S0169-1368(15)00127-4
DOI: doi: 10.1016/j.oregeorev.2015.05.005
Reference: OREGEO 1512

To appear in: *Ore Geology Reviews*

Received date: 6 March 2015
Revised date: 3 May 2015
Accepted date: 6 May 2015

Please cite this article as: Duchesne, Jean-Clair, Liégeois, Jean-Paul, The origin of nelsonite and high-Zr ferrodiorite associated with Proterozoic anorthosite, *Ore Geology Reviews* (2015), doi: 10.1016/j.oregeorev.2015.05.005

This is a PDF file of an unedited manuscript that has been accepted for publication. As a service to our customers we are providing this early version of the manuscript. The manuscript will undergo copyediting, typesetting, and review of the resulting proof before it is published in its final form. Please note that during the production process errors may be discovered which could affect the content, and all legal disclaimers that apply to the journal pertain.

ACCEPTED MANUSCRIPT

The origin of nelsonite and high-Zr ferrodiorite associated with Proterozoic anorthosite

Jean-Clair Duchesne[1,*] & Jean-Paul Liégeois[2]

[1]Department of Geology, University of Liège, Bat. B20, B-4000 Sart Tilman, Belgium

[2] Geodynamics and Mineral Resources, Royal Museum for Central Africa, B-3080 Tervuren, Belgium

*corresponding author

10 718 words (71270 charac. including space)

6 tables

10 figures

100 references

corresponding author: Prof. Jean-Clair Duchesne

e-mail: jc.duchesne@ulg.ac.be

tel.: +32477496963

ACCEPTED MANUSCRIPT

ACCEPTED MANUSCRIPT

Abstract

A petrological and geochemical (major and trace elements, Sr-Nd isotopes) study of two nelsonite occurrences (the Kydlandsvatn and Hestnes deposits) in the Rogaland anorthosite province (Southern Norway) reveals that both deposits are cumulates but were generated from strikingly different magmas and processes. The Kydlandsvatn deposit was formed from a primitive jotunite similar to the Bjerkreim-Sokndal parental magma by crystal accumulation. By contrast, the Hestnes cumulate, with high REE and Zr contents, negative Eu anomaly, Cr-rich magnetite, Nb-rich ilmenite and high Nb/Ta and Zr/Hf whole-rock ratios appears to result from the crystallization of an immiscible Fe-rich and Si-poor melt under highly oxidized conditions. Other jotunites/ferrodiorites with high Zr-contents are typically associated with anorthosites in the Rogaland, Laramie and Adirondacks anorthosite complexes. In Rogaland, they also have an identical Sr-Nd isotope signature as the Hestnes nelsonite. These high-Zr jotunites cannot have been produced through extreme differentiation of ordinary jotunite magmas. Their formation from direct melting of a crustal source or assimilation of a nelsonite cumulate is highly unlikely. Occurrence of a high-Zr jotunite at the margin of a quartz mangerite dyke is evidence that immiscibility takes place, though furtively, along the jotunite liquid line of descent. It is suggested here that high-Zr jotunites in dyke rocks or parental to high Zr-nelsonites resulted from fractional crystallization of a Fe-rich immiscible melt formed at higher pressures in the polybaric evolution of anorthosites, conditions that are not yet explored experimentally.

Keywords: Rogaland anorthosite province, Fe-Ti deposits, layered intrusion, jotunite, ferrodiorite, immiscibility

ACCEPTED MANUSCRIPT

ACCEPTED MANUSCRIPT

1. Introduction

Extreme differentiation of tholeiitic melts generally yields apatite and Fe-Ti oxide bearing cumulates as recorded in layered intrusions (e.g. Namur et al., 2010; Tegner et al., 2006). Fe-Ti-P-rich gabbronorites are also common members of the AMCG (Anorthosite, Mangerite, Charnockite, Granite) suite and result from the differentiation of parental jotunite (ferrodiorite) melts (e.g. Duchesne et al., 1989; Mitchell et al., 1996; Vander Auwera et al., 1998b; Wilson et al., 1996). Nelsonites are Fe-Ti-oxide-apatite rocks. They can be considered as a particular type of Fe-Ti oxide-apatite rocks formed by strong crystal sorting during accumulation of liquidus phases (Charlier et al., 2015; Charlier et al., 2009; Charlier et al., 2008; Dymek and Owens, 2001; Tollari et al., 2008). On the other hand, the seminal work of Philpotts (1967) has revealed that liquid immiscibility is another potential mechanism of formation of nelsonite and more generally of Fe-Ti deposits (Chen et al., 2013; Force, 1991; Kolker, 1982; Wang and Zhou, 2013; Zhou et al., 2015). The high liquidus temperature ca. 1400°C of apatite-ilmenite melts is nevertheless a major obstacle to this hypothesis as pointed out by Lindsley (2003), and decisive experimental data are lacking to support this hypothesis. However, considering that temperatures >1100°C (e.g. 1150°C in Sri Lanka; Sajeev & Osanai, 2004) are recorded in continental crustal metamorphic terranes (Kelsey & Hand, 2014 and references therein), it is reasonable to envisage that even higher temperatures can occur at the continental crust/mantle boundary, especially in favourable conditions (e.g. in crustal tongues; Duchesne et al., 1999).

Liquid immiscibility is known to take place during the differentiation of tholeiitic melts (Charlier and Grove, 2012; Dixon and Rutherford, 1979; Philpotts, 1982; Veksler and Charlier, 2015) with production of conjugate Fe-rich and Si-rich melts. This process has been proposed as a viable mechanism to explain a well-defined Daly gap (i.e. absence of intermediate liquid compositions) when the conjugate immiscible melts are segregated at a large scale (Charlier et al., 2013). If, in contrast, the two melts form an emulsion, this gap is recorded in the composition of erupted lavas. Since the Fe-rich melts are also enriched in Ti and P, their crystallization in a plutonic environment can potentially give rise to nelsonitic cumulates. However, because the two immiscible liquids are generally kept in equilibrium along the bimodal surface, the liquidus phases of the two conjugate melts have the same composition (Bowen, 1928), which makes it very difficult to distinguish between a cumulate formed by crystallization of an immiscible Fe-rich melt and a cumulate formed in an homogeneous liquid. If immiscibility does not occur, mineral compositions produced from a

ACCEPTED MANUSCRIPT

homogeneous melt would also be the same. In the Sept Iles intrusion, the immiscibility is recorded in the crystallization products through a highly bimodal distribution in the proportion of cumulus minerals (Charlier et al., 2011; Namur et al., 2012). However, without direct evidence for the presence of two immiscible melts in inclusions trapped in apatite (Charlier et al., 2011) these variations in modal proportions would probably have been interpreted as the result of efficient crystal sorting within the main magma body or at the top of the crystal mush. In the Skaergaard intrusion, melt inclusion studies demonstrated that a significant part of the intrusion crystallized from an emulsion of Fe- and Si-rich immiscible melts (Jakobsen et al., 2005, 2011). At the top of the Bushveld Complex, REE abundances in apatite were considered as resulting from crystallization in an immiscible liquid by Van Tongeren and Mathez (2012, 2014) whereas this hypothesis was debated by Cawthorn (2013, 2014).

This significant issue of distinguishing cumulate rocks produced from immiscible melts as opposed to cumulates produced from the crystallization of tholeiitic homogeneous magmas is addressed in this work. Two different types of nelsonite occur in the Rogaland anorthosite province (RAP) and can be discriminated using the geochemical characteristics of the bulk ores and their mineral compositions (magnetite, ilmenite and apatite). The first type has strong similarities with cumulates in the neighbouring Bjerkreim-Sokndal (BKSK) layered intrusion which was shown to result from fractional crystallization of primitive jotunites. The second type of nelsonite strongly differs from the first one by the high REE content of apatite, the presence of zircon in the rocks and the Cr-rich nature of the liquidus magnetite. These could potentially result from the crystallization of an unusual type of jotunite, with high Zr and REE contents that are known to occur within the RAP and other anorthosite provinces. Crystallization from a Fe-rich immiscible melt is another possibility for the origin of these rocks (Namur et al., 2012). In this work, we focus on a high-Zr jotunite occurring as a contact rock in a quartz mangeritic dyke. These rocks are compositionally similar to Fe-rich immiscible liquids produced experimentally at low to intermediate pressure. We thus suggest that they result from the crystallization of a Fe-rich immiscible melt. We finally propose that high-Zr jotunites occurring in dykes are also immiscible melts formed at higher pressure in the polybaric evolution of massive anorthosites and that high-Zr nelsonites are cumulates formed from this Fe-rich immiscible melt.

ACCEPTED MANUSCRIPT

2. Geological framework

2.1 The Rogaland anorthosite province

The Rogaland anorthosite province (RAP) in South Norway is a typical AMCG (Anorthosite-Mangerite-Charnockite-Granite) province emplaced at the end of the Sveconorwegian orogen at ca. 930 Ma (Schärer et al., 1996) into Mesoproterozoic high-grade (granulitic) metamorphic gneisses. Three large massif-type anorthosites, namely the Egersund-Ogna (EGOG), the Håland-Helleren and the Åna-Sira massifs, together with the Bjerkreim-Sokndal (BKSK) layered intrusion and its Apophysis are the main intrusive bodies of this AMCG province (Fig. 1). The anorthosite massifs are interpreted as resulting from diapiric intrusion of a mush of crystals formed by polybaric crystallization in a gradient of pressure from 11-13 kbar to 4-5 kbar (Charlier et al., 2010a; Duchesne et al., 1985b; Longhi et al., 1999; Maquil and Duchesne, 1984) in post-collision conditions along pre-existing lithospheric weakness zones (Duchesne et al., 1999). The EGOG massif has a foliated leuconorite inner margin made up of a mush formed at ca. 7 kbar from high-alumina basalt. This margin was deformed by the intrusion of the less deformed anorthositic inner part that crystallized from several batches of ferrodioritic magma (Charlier et al., 2010a). The Helleren massif is also deformed and foliated and was intruded by the Håland massif, a body very similar to the Åna-Sira massif (Duchesne et al., 1985b).

The BKSK intrusion comprises a 7 km-thick layered series of cumulates associating anorthosite, troctolite, leuconorite, norite, and gabbronorite (Wilson et al., 1996; and references therein) overlaid by acidic rocks (mangerite, quartz mangerite and charnockites) (Duchesne and Wilmart, 1997) that extend into the Apophysis (Bolle and Duchesne, 2007). Chilled margins of the intrusion permit to define the parental magma as a jotunite (hypersthene ferrodiorite) (Duchesne and Hertogen, 1988; Robins et al., 1997), the composition of which was later referred to as a primitive jotunite (Vander Auwera et al., 1998b). Experimental work confirmed that this parental magma gave rise to the succession of cumulates observed in the intrusion (Vander Auwera and Longhi, 1994; Vander Auwera et al., 1998b).

2.2 The jotunite dyke system

A system of jotunitic dykes cuts across all massifs (e.g. the Vettaland, Varberg or Lomland dykes) (Duchesne et al., 1985a; 1989) (Fig. 1). The Tellnes dyke in the Åna-Sira massif varies in composition along strike from jotunite to mangerite (hypersthene monzonite), quartz mangerite (hypersthene quartz monzonite) and charnockite (hypersthene granite) (Wilmart, 1988; Wilmart et al., 1989). The jotunitic rocks in the RAP have been subdivided into two

ACCEPTED MANUSCRIPT

main types according to their major and trace element geochemistry (Vander Auwera et al., 1998b): (1) the primitive jotunites, parent namely to the BKSK layered intrusion (Duchesne and Hertogen, 1988; Robins et al., 1997), and (2) the evolved jotunites which occur in the jotunitic dykes system (Vander Auwera et al., 1998b). Their average compositions are reported in Table 1. Compared to the primitive jotunites, the evolved jotunites have a lower Mg# and are richer in P_2O_5 and REE, but also display Eu/Eu* ratio close to unity, the other elements being similar within statistical and natural variations. All compositions in the jotunite dyke system and particularly the chilled rocks define a continuous liquid line of descent from primitive jotunite to charnockite (Vander Auwera et al., 1998b).

2.3 The high-Zr jotunite

Among all rock types that occur in the RAP jotunite dyke system, a rare lithology, representing some 10% of the analysed jotunitic samples, has been identified (Bolle et al., 2003; Bolle and Duchesne, 2007; Duchesne et al., 1989; Wilmart et al., 1989). Compared to primitive and evolved jotunites, it is characterized by significantly higher Zr-Hf (5 to 11 times) and REE (3 to 6 times) contents and, usually, by a strong negative Eu anomaly (Eu/Eu*= 0.34) (Table 1). This lithology occurs in thin dykes which can be satellite to larger dykes, such as the Tellnes dyke (Duchesne et al., 1989; Wilmart, 1988; Wilmart et al., 1989)], the Sirevåg dyke (sample #75-54-2), satellite to the Vettaland dyke (Duchesne et al., 1989), dykes satellite to the Apophysis (Bolle, 1998; Bolle et al., 2003), or independent dyke, such as the Løyning dyke (sample #76-27) (Figs 1 & 2). These compositions represent melts as evidenced by chilled structures without phenocrysts (Duchesne et al., 1989; Wilmart et al., 1989).

A peculiar occurrence of high-Zr jotunite is a 5-cm-thick fine-grained margin (sample #78-32-2) of the Tellnes dyke at Botnevatn (Fig. 1) where the main dyke rock is a quartz mangerite (#78-32; Wilmart, 1988; Wilmart et al., 1989). The margin has the same mineralogy and mineral compositions as the quartz mangerite within the dyke but is richer in modal proportions of mafic minerals (pyroxenes, opaques, apatite and zircon). Interestingly, the petrographic texture of the quartz mangerite is similar to that described by Philpotts (1981) in some quartz mangerites from southern Quebec. The mafic minerals (inverted pigeonite, iron-rich augite, Fe-Ti oxides and minute grains of apatite and zircon) form clusters between larger grains of quartz and mesoperthite. According to Philpotts (1981) these clusters have crystallized from droplets of immiscible Fe-rich melts trapped in the Si-rich melt.

High-Zr jotunite/ferrodiorite also occurs in the Laramie anorthosite complex (LAC) and in the Adirondacks anorthosite province (AAP): three high-Zr ferrodiorites are reported

ACCEPTED MANUSCRIPT

by Mitchell et al. (1996) and two monzonites by Scoates and Chamberlain (2003) in the LAC, and a high-Zr mangerite occurs at Lake Placid in the AAP (Seifert et al., 2010). The compositions of these 6 high-Zr rocks are reported in Table 1. Fe-Ti-Zr-REE rich melt bands occur in the Bolangir anorthosite pluton (East India) (Nasipuri et al., 2011). This peculiar rock is interpreted as residual melts from the anorthosite crystallization that have been contaminated by crust-derived zircon grains (Nasipuri et al., 2011). The high REE concentrations (up to 5700 ppm) and low Eu/Eu* (down to 0.13) ratios are nevertheless similar to the high-Zr rocks considered here.

2.4 The Fe-Ti deposits in the norito-charnockitic

The province hosts a number of Fe-Ti deposits (Duchesne, 1999; Schiellerup et al., 2003), including the world class Tellnes body (Charlier et al., 2006; and references therein). The present work focuses on some of the Fe-Ti ore bodies, now abandoned from mining, south of Egersund (Fig. 2), as well as on some dyke rocks belonging to the jotunite dyke system.

The ore-bodies studied in this work are located in a zone at the vertical contact between the EGOG and the Helleren massifs (Fig. 2). The anorthosite and leuconorite of both massifs are foliated parallel to the contact. A septum of strongly deformed banded gneiss associating charnockitic and noritic lithologies, formerly called the "Zone norito-granitique" by Michot (1960), is wedged in the contact. To the west of this zone, the Løyning mafic body intruded in the foliated margin of the EGOG massif, parallel to the foliation, and was deformed together with the margin (Vander Auwera et al., 2006). Another mafic intrusion, further to the east, the Koldal body, also emplaced in this zone, but after the main deformation occurred as shown by crosscutting contacts with the foliated marginal rocks (Vander Auwera et al., 2006). These magmas are interpreted as dense residual melts drained through the anorthositic crystal mush along sloping structures of the diapirs (Vander Auwera et al., 2006). Small Fe-Ti deposits of various extensions from meter- to hundred meters in size are located in the Helleren massif and straddle the contact zone with the EGOG body or with the banded gneiss septum. From East to West, there are the Kydlandsvatn deposit, the Kaknuden vein, the Rødemyr vein and lens, and finally the Hestnes and Egersund deposits (Fig. 2). These occurrences were first reported by Hubaux (1960) and later documented by Roelandts and Duchesne (1979). These deposits are interpreted as concentrations of Fe-Ti oxide minerals formed in, or drained from, layered magma chambers marginal to the Helleren diapir and emplaced in the vertical zone of weakness between the EGOG and Helleren massifs.

We focus on two occurrences of nelsonitic rocks that belong to the Kydlandsvatn and Hestnes deposits.

ACCEPTED MANUSCRIPT

3. The Kydlandsvatn and Hestnes deposits

3.1 Structure and petrography

The Kydlandsvatn deposit is made up of almost vertical (70°S) veins of Fe-Ti oxide ore passing on strike to ilmenite norite or to an association of layers of ore and anorthosite or leuconorite (Fig. 3A). The strongly dipping position, as also observed in the Løyning mafic body, results from the tilting of a magma chamber due to the diapirism of the EGOG and Håland massifs. In the Kydlandsvatn deposit, the most common ore type is made up of hemo-ilmenite (Hem_{20}) + hercynitic spinel ± Ti-poor magnetite + traces of sulphides, plagioclase (An_{40-48}) and hypersthene. Locally, nelsonite may form homogeneous veins of lenses comprising the same mineral assemblage as in the ore, plus variable amount of apatite (up to 26 vol.%) (Fig. 3B).

The Hestnes deposit and its neighbour the Egersund deposit (Fig. 2) intruded the Håland massif close to the contact with the septum of norito-charnockitic gneiss. Both deposits are made up of nelsonite. The Egersund deposit has now disappeared due to a recently built factory, while in Hestnes some outcrops are still accessible, although tailings are the main source for sampling. The dominant ore is a heterogeneous nelsonite where the apatite content, the grain size and the structure of the ore can be highly variable. The latter can be homogeneous at sample scale, or modally layered on a centimetre to decimetre scale (Fig. 4A).

The net-textured oxide minerals are Al-spinel and Ti-rich magnetite and homogeneous ilmenite (Fig. 4D). The magnetite is characterized by two generations of Al-spinel exsolutions and cloth and trellis oxy-exsolutions of ilmenite. Reaction rims at the contact between magnetite and ilmenite (Duchesne, 1972) are absent or very thin. Both oxide minerals have variable grain size from layer to layer and can coalesce into 1-2 cm long and 2-4 mm wide "platy" grains. Magnetite is the only main mineral in coarse-grained layers (Fig. 4A). Apatite varies in length from 0.5 mm to 5 mm with aspect ratio up to 1/10. Its proportion is highly variable and changes from 50 vol.% down to zero. It is elongated parallel to the layering and, together with other phases, contributes to the overall cumulate structure. Sulphides are remarkably abundant in the coarse-grained rocks dominated by magnetite. Interstitial plagioclase (An_{31-37}), orthopyroxene (En_{40-50}), some quartz and rare but large zircon crystals (Fig. 4C) are interpreted as the crystallization products of a quartz dioritic interstitial liquid. This liquid is particularly abundant in the contact zone with the country-rocks where it crystallized, in addition to other phases, spectacular zircon crystals (Fig. 4B), similar to those

ACCEPTED MANUSCRIPT

reported in a nelsonite body from the Montpelier anorthosite, Virginia (Aleinikoff et al., 1996).

3.2. Rocks and minerals elemental compositions

Major and trace element bulk-rock (Table 2) and mineral (Tables 3 and 4) compositions of selected samples were determined by X-ray fluorescence and ICP-MS (see details on the analytical protocols in the appendix). Due to the complex intergrowths in the Fe-Ti oxide minerals, electron microprobe could not be used for analysing the bulk compositions of these minerals. Instead, the minerals were separated by magnetic and dense liquid methods before being analysed by X-ray fluorescence. Major elements and Cr, Zn, V, Co, Ni, Nb and Zr analyses of Fe-Ti oxides are given in Table 3. Apatite grains were also separated and measured for REE compositions by ICP-MS (Table 4).

The Kydlandsvatn hemo-ilmenite is rich in Mg, Fe^{3+} ($Ilm_{84-85}Hem_{16-15;}$ calculated from total FeO using Andersen et al., 1993) and V and the magnetite is relatively poor in Ti and rich in V and Cr. When coexisting, both minerals have undergone subsolidus equilibration down to relatively low temperatures (~600°C; Table 3). At Hestnes, the ilmenite is close to the pure ilmenite end-member ($Ilm_{99-95}Hem_{1-5}$) of the ilmenite-hematite solid solution and is particularly rich in Nb and Zr; the magnetites are Ti-rich with some variations between 7 and 10 wt% TiO_2, corresponding to 22 to 32 mol.% Usp in solid solution. The V concentrations are relatively constant but Cr varies notably within the range from 0.02 to 0.27 wt.% Cr_2O_3. The subsolidus equilibrium temperatures are also relatively low (400° to 650°C) (Table 3).

The bulk compositions of the rock samples (Table 2) show a large variation of the P_2O_5 content of the nelsonite samples in both deposits, corresponding to 6 to 20 wt.% apatite in Kydlandsvatn and to 2 to 50 wt.% apatite in Hestnes. In the latter deposit, there is a marked decrease in the apatite content with increasing sample grain size.

The bulk sample composition allowed us to determine the relative proportion of mineral phases. For instance, in sample #00-15, the modal composition is 16% magnetite + 64% ilmenite + 3% spinel + 15% apatite + 2% plagioclase (An_{40}); in sample #00-41, 44% magnetite + 16% ilmenite + 29% apatite + 4% plagioclase (An_{34}) + 7% orthopyroxene (En_{41}). The mineralogical variability is compositionally illustrated by inter-element relationships in Fig. 5, which allow us discriminating between Hestnes and Kydlandsvatn. The bulk-rock Ce (and REE) concentrations are controlled by the composition and modal proportion of apatite (Fig. 5a). The REE compositions in apatite from both deposits are reported in Table 3 and plotted in the chondrite-normalized diagram of Fig. 6. The average Nb/Ta ratio in Hestnes (37) is higher than in Kydlandsvatn (18) and Nb attains maximum values in Hestnes (Fig. 5b).

ACCEPTED MANUSCRIPT

The Cr and Zn concentrations are very variable in Hestnes due to variations in the magnetite compositions (Figs 5d and e). The V concentrations in Kydlandsvatn are higher than in Hestnes due to high values in both Fe-Ti oxide minerals (Fig. 5c). The Cu/Ni ratios are different in the two occurrences reflecting different sulphide associations (Fig. 5f). Finally the Zr concentrations are very variable in Hestnes compared to Kydlandsvatn and this can be due to variable amounts of ilmenite and to a possible nugget effect (Fig. 5g).

3.3. Isotopic compositions of apatite from Fe-Ti deposits

Rb-Sr and Sm-Nd isotopic compositions of apatite separates from the Kydlandsvatn and Hestnes nelsonites and from the Kaknuden and Rødemyr deposits are reported in Table 5. The analytical methods are described in appendix. The values of the ε_{Nd} and $^{87}Sr/^{86}Sr$ at 930 Ma, the age of the RAP (Schärer et al., 1996), are plotted in Fig. 7 together with data of Bolle et al. (2003) on primitive and evolved jotunites, on high-Zr jotunites and on acidic rock from the BKSK intrusion and Apophysis. Bolle et al. (2003) have defined two trends of evolution, linking by binary mixing the most primitive jotunite to two crustal components C1 and C2. This expresses contamination processes combined to fractional crystallization with an Rb-enriched Pre-Sveconorwegian basement of southernmost Norway and an Rb-depleted deep continental crust component, respectively. Interestingly, the Kydlandsvatn, Kaknuden and Rødemyr ores follow the trend towards C2, and the Hestnes nelsonites as well as the high-Zr jotunites follow the trend towards C1. This is an additional character emphasizing the distinction between the two types of nelsonites already revealed by the trace element contents of apatite and whole rocks.

3.4. Oxygen fugacity of the Hestnes melt

Information on the fO_2 conditions that has controlled the Hestnes and Kydlandsvatn formation and subsolidus evolution can be obtained by considering the Fe-Ti oxide mineral compositions (Table 3). Application of the two-oxide geothermometry calculated by the QUILF algorithm (Andersen et al., 1993) shows that equilibrium between the two oxides was maintained in the subsolidus evolution down to low temperatures. Assuming a 1100°C-1200°C range of liquidus temperatures in the jotunite magma by analogy with experimental data (Vander Auwera and Longhi, 1994; Vander Auwera et al., 1998b) in which the Kydlandsvatn cumulate has formed, the ilmenite compositions of samples #00-15 and #79-17-1 (Table 2), following the experimental approach of Lattard et al. (2005), indicate fO_2 conditions between ΔFMQ= 0 and -0.8. In Hestnes, reaction rims between magnetite and ilmenite which are produced in the subsolidus evolution (Duchesne, 1972; Frost and Lindsley,

ACCEPTED MANUSCRIPT

1992; Frost et al., 1988) are very rare or absent and no external granule exsolutions of ilmenite is observed. In sample #00-41, magnetite (45 wt%) dominates ilmenite (16 wt%), and this suggests that ilmenite was the only oxide to change its composition in the inter-oxide re-equilibration (Frost et al., 1988). In other words, the fO_2-T conditions would have followed the magnetite isopleth during cooling. In the 1100°C-1200°C range of liquidus temperatures, the fO_2 conditions can be determined from the T- fO_2 grid for coexisting magnetite-ilmenite pairs, based on the solution model of Spencer and Lindsley (1966). For sample #00-41, ΔFMQ values > +2.8 are obtained and are *higher* than in the Kydlandsvatn deposit. This conclusion is in agreement with experiments on the stability fields of Fe-Ti oxides (Snyder et al., 1993; Toplis and Carroll, 1995), which show that oxidizing conditions favour the early appearance of Ti magnetite as well as immiscibility (Naslund, 1983; Vicenzi et al., 1994).

4. Discussion

4.1. Nelsonite are cumulates not liquids

In Hestnes, nelsonites show a striking evidence for gravity driven accumulation such as modally and grain size graded layers of Fe-Ti oxide minerals and conspicuous planar orientation of apatite. Accordingly whole-rock compositions are variable (Table 2). The variable proportions of apatite (from zero to 50 wt.%) preclude a liquid with eutectic composition as proposed by Philpotts (1967). The net texture of the ore does not result from crystallisation of a liquid, as proposed by Naldrett (2004) for sulphides, but from subsolidus recrystallization of Fe-Ti oxide minerals (Duchesne, 1996, 1999). In Kydlandsvatn, the nelsonites are homogeneous at sample scale but occur in close association with apatite-free samples containing Fe-Ti oxides of the same composition. In the field, layered structures associating anorthosite and Fe-Ti oxides bands are observed (Fig. 3). Major element compositions in both deposits are also quite distinct from Fe-rich liquids obtained experimentally (Charlier and Grove, 2012; Dixon and Rutherford, 1979) or measured on immiscible globules in volcanic rocks (Philpotts, 1982). The nelsonites investigated here are thus not liquids but cumulates.

4.2. Similarities between the Kydlandsvatn nelsonite and the Bjerkreim-Sokndal mafic cumulates

The BKSK layered intrusion results from the differentiation of a parental magma of jotunitic composition (Duchesne and Hertogen, 1988; Robins et al., 1997). Following the nomenclature of Irvine (1982) (with p= plagioclase, h= orthopyroxene, i= ilmenite, m= magnetite, a= apatite, o= olivine, c= clinopyroxene, -C= cumulate), the sequence of crystallization comprises three major types of cumulate represented by leuconorite (phi-C and phim-C),

ACCEPTED MANUSCRIPT

gabbronorite (phimac-C) and jotunite (poima-C). Brief episodes with poim-C (e.g. in the Storeknuten section), and pi-C also occur before the leuconorite stage (Charlier et al., 2005; Duchesne and Charlier, 2005; Duchesne and Hertogen, 1988; Wilson et al., 1996: and references therein). The transition between the leuconorite and gabbronorite takes place when the fraction of liquid is close to 0.5 (Duchesne, 1978; Vander Auwera et al., 1998b). The Fe-Ti oxide minerals (Duchesne, 1972) pass from hemo-ilmenite ± magnetite in the leuconorite stage to ilmenite + Ti-rich magnetite (up to the top of the jotunite stage) with a strong decrease in the concentration of compatible elements (Cr, V, Ni) particularly well marked in magnetite. From 1.46% Cr_2O_3 in the magnetite of the leucotroctolite (poim-C), the Cr concentration decreases rapidly upwards in the leuconorite phase and remains <20 ppm (limit of detection) in the gabbronorite phase (Duchesne, 1972; Jensen et al., 1993). Apatite from the beginning of the gabbronorite stage to the end of the jotunite stage shows an increase in the REE concentrations by a factor of ca. 2 (Fig. 6) (Charlier et al., 2005).

The similarities between the Kydlandsvatn nelsonites and the BKSK cumulates are conspicuous: the REE concentrations in apatite plot within the range of BKSK apatite (Fig. 6). The association of the Fe-Ti oxides (hemo-ilmenite ± magnetite) and the Cr and V contents in the nelsonite Fe-Ti oxides match those at the beginning of the BKSK leuconoritic trend. This strongly suggests that the Kydlandsvatn nelsonite were also crystallized from a jotunitic magma. The latter, however, was not exactly similar to the BKSK parental magma (the so-called Tjørn chill of Vander Auwera and Longhi, 1994) but somewhat richer in Ti and P to account for early crystallization at the liquidus of apatite and the large amount of ilmenite compared to orthopyroxene. Such characteristic of jotunitic melts is nevertheless frequently observed in Fe-Ti deposits related to massif-type anorthosites (Charlier et al., 2006; Charlier et al., 2015; Charlier et al., 2010b; Charlier et al., 2008). In conclusion, the Kydlandsvatn nelsonite is a cumulate formed from a jotunitic magma.

4.3. Parental magmas to Kydlandsvatn and Hestnes deposits are distinct

Could the contrasted hallmarks between Hestnes and Kydlandsvatn nelsonites result from a fractional crystallization (FC) process similar to that in BKSK?

There are evidences compatible with a FC: (1) the Fe-Ti oxide mineral association in the BKSK sequence is first hemo-ilmenite ± Ti-poor magnetite, as in Kydlandsvatn, that passes upwards to Ti-rich magnetite + ilmenite, as in Hestnes; (2) the REE concentrations in apatite increase upwards in BKSK. But more other evidences are incompatible with a FC process: (1) modelling of the gabbronorite whole-rock composition has revealed that the crystallization of the apatite in BKSK buffered the REE evolution in the melt (Charlier et al.,

ACCEPTED MANUSCRIPT

2005); thus, the REE content of the apatite cannot increase well above the value attained in the upper part of the gabbronorite stage (Fig. 6), which is well below the REE concentrations of the Hestnes apatite; (2) fractional crystallization in the BKSK intrusion led to a drastic decrease of the Cr concentration in the magma as revealed by the evolution of Cr in magnetite (Duchesne, 1972); if the Hestnes deposit fractionated from the same magma as the Kydlandsvatn deposit, it should contain a magnetite very poor in Cr, which is not the case, the magnetite in Hestnes is strongly enriched in Cr (up to 2690 ppm Cr_2O_3, Table 2); (3) the Hestnes ilmenites have five times more Nb (189 to 227 ppm) than the Kydlandsvatn ilmenites (42 to 46 ppm) (Table 3); the latter values are similar to those of the ilmenite in the less evolved BKSK cumulate (poim-C) (29-39 ppm; Duchesne, unpublished data); accepting the conservative hypothesis that the Kydlandsvatn nelsonite corresponds to the gabbronoritic stage of BKSK, the constancy in Nb concentrations in ilmenite implies that the bulk partition of Nb remained close to unity in the process, which precludes an increase up to the values observed in the Hestnes ilmenite; (4) the different Sr-Nd isotope signatures in apatite (Fig. 7) in the Kydlandsvatn and Hestnes nelsonites impose two different sources and so two different magmas. We can conclude that the Kydlandsvatn and Hestnes nelsonites were formed in two different magmas and, as shown above, under different fO_2 conditions.

Could the contrasted apatite REE distributions between Kydlandsvatn and Hestnes be due to a trapped liquid shift effect as proposed e.g. by Cawthorn (2013) in the Bushveld Complex? The four-fold increase observed here would require an amount of trapped liquid that is not supported by the whole-rock concentration in incompatible elements such as Si, Na, K, Rb and Ba that remain in the same range of values in both deposits (Table 2). In addition, as written above, Sr and Nd isotopes impose two different magmas and sources and cannot be explained with a trapped liquid generated within the same magma as the cumulative nelsonite. This hypothesis simply does not work here.

4.4. Producing the Hestnes magma through an immiscibility process

High REE values in the Hestnes whole rocks and apatites coexist with high values of Cr in magnetites, which is paradoxical. Indeed, REE and Cr have usually very contrasted behaviours in fractionating magmas, the first elements being incompatible and the second being highly compatible. This apparent paradox leads us to consider that the magma in which the Hestnes cumulate formed was a Fe-rich liquid resulting from an immiscibility process. Indeed, the pioneering experimental work of Watson (1976) has shown that the REE and Cr are readily enriched by factors 4-5 and 3.0-3.3 respectively in Fe-rich melts. For the REE, this behaviour was later confirmed by a number of studies (Green, 1994; Ryerson and Hess, 1978;

ACCEPTED MANUSCRIPT

Schmidt et al., 2006; Veksler et al., 2006; Vicenzi et al., 1994) and for Cr an enrichment by a factor ca. 4 was measured by Schmidt et al. (2006). As qualitatively predicted by Ryerson and Hess (1978), Eu^{2+} and Sr have similar behaviours in both immiscible melts, and the REE^{3+} are strongly enriched in the Fe-rich liquid while the partitioning of Sr, and thus of Eu^{2+}, is close to unity (Green, 1994). It thus comes that, relative to the other REE, Eu^{2+} will significantly decrease in the Fe-rich liquid, which is observed in the apatite REE distribution in Hestnes (strong negative Eu anomaly) compared to Kydlandsvatn. Zr and Nb are more enriched in the Fe-rich melt than their diadochic elements Hf and Ta (Green, 1994; Schmidt et al., 2006; Vicenzi et al., 1994) implying higher Zr/Hf and Nb/Ta ratios. This is observed in Hestnes (average whole-rock ratios: Zr/Hf= 43 ± 4, Nb/Ta= 37 ± 9) compared to Kydlandsvatn (Zr/Hf= 34 ± 2, Nb/Ta= 18 ± 3). On the other hand, experiments show that Th/U ratios are similar in immiscible pairs of melts (Schmidt et al., 2006), which is observed here: Th/U = 0.9 ± 0.2 in Hestnes whole-rocks and 1.4 ± 0.3 in those of Kydlandsvatn. All these features favour an immiscible nature of the Hestnes melt. However, reconstructing the accurate composition of the melt with which the Hestnes cumulate has equilibrated to identify the mechanism of melt formation is not possible. Indeed, the crystal-melt partition coefficients strongly depend on the structure and composition of the melt and this dependence is not quantitatively determined for individual minerals.

Interestingly, the high REE contents with a strong Eu negative anomaly of the apatite of the top of the Bushveld Complex (Van Tongeren and Mathez, 2012), in contrast with the much lower REE abundance and Eu anomaly of apatite stratigraphically below, can be taken as evidence that the magma that has crystallized the top sequence was different from the resident magma and that immiscibility may have played a role in its formation. Our data on the Hestnes deposit leads us, however, to interpret the REE-rich apatite of the Bushveld as being formed in a Fe-rich melt rather than in the Si-rich melt proposed by Van Tongeren and Matthez (2012). Similarly the same REE distribution in apatite from the Lepuchovo nelsonite (Poland; Duchesne, unpublished data) supports the interpretation of Kozlowski and Wiszniewska (2001) that this nelsonite resulted from an immiscibility process. High REE content in the apatite of the Port Leyden nelsonite (Darling and Florence, 1995) and large zircon crystals in the Montpelier nelsonite (Aleinikoff et al., 1996) suggest that these nelsonites could have been produced by the same process as the Hestnes deposit.

ACCEPTED MANUSCRIPT

4.5. The origin of high-Zr jotunite trends and the Hestnes parental melt

The Sr-Nd isotope signature of the Hestnes deposit (Fig. 7) and the occurrence in the Hestnes ore of zircon grains and apatite with high REE concentrations and low Eu/Eu* point to a possible relationship with high-Zr jotunite.

Relationships between major elements and Mg# in the high-Zr jotunites/ferrodiorites identified in the RAP, LAC and AAP (Table 1) are illustrated in Fig. 8 and compared to the RAP jotunite liquid line of descent (LLD) which has been defined by chilled rocks and by the Tellnes dyke rocks (Vander Auwera et al., 1998b). It can be seen that the Mg# of the RAP vary from 0.24 to 0.13 and in the LAC from 0.19 to 0.05. In the RAP, the high-Zr rocks grossly form trends superimposed to the jotunite LLD for TiO_2, Fe_2O_{3t}, MgO and P_2O_5, sub-parallel but below the LLD for K_2O, and above for Al_2O_3, CaO, and Na_2O. The trends in the LAC are distinct from the RAP trends but sub-parallel or steeper. Two rocks significantly differ from the other high-Zr jotunites, sample #78-32-3 (the Tellnes dyke fine-grained margin) in the RAP and sample #PM-618 in the LAC: they are lower in alkalies, SiO_2 and Al_2O_3 and higher in TiO_2 and P_2O_5. Some trace elements clearly contrast the high-Zr jotunites from the RAP LLD (Fig. 9). Not only the Zr content is much higher (specially in #78-32-3) than in the LLD, but also the REE are much enriched with a strong negative anomaly (the exception is sample #MPK60a in the LAC that is probably a melt laden with feldspars because anomalously rich in Sr and Ba, Table 1). The $[Ce/Yb]_N$ ratios are not significantly different in the high-Zr jotunites from that in the LLD.

The gross parallelism of the RAP and LAC high-Zr trends with the jotunite LLD points to a similar fractionation process to that described for the evolved jotunite in Vander Auwera et al. (1998b). In the RAP the compositions of the most primitive high-Zr jotunites cannot result from fractional crystallization of evolved jotunites because they display the same Mg# and in such process the buffering role of apatite would have prevented the increase in REE in the melt, as discussed above. In the LAC, it has been argued that the high-Zr ferrodiorite represent products of extreme fractionation of common ferrodiorites (Mitchell et al., 1996), but, again, this hypothesis does not account for the buffering effect of saturation in apatite on the REE content and saturation in Fe-Ti oxides on the Fe content.

We are thus forced to envisage an origin different from that of the primitive and evolved jotunites. More generally, the origin of the jotunite melts is still debated. Following Emslie (1978), jotunites (or ferrodiorites) are residual melts derived from basaltic magmas after formation of anorthosites in a deep-seated magma chamber (see Mitchell et al., 1996; Scoates et al., 1996; and references therein). On the other hand, following a proposition of

ACCEPTED MANUSCRIPT

Duchesne et al. (1989), it has been shown experimentally that jotunites could be derived from partial melting of gabbronoritic rocks in the crust (Longhi, 2005; Longhi et al., 1999). With the first process, the formation of high-Zr melts would require extreme degrees of fractionation not compatible with relatively low Mg#, and, with the second process, very unusual source rock compositions. We therefore consider that both processes are very unlikely if not impossible for the generation of high-Zr jotunites.

Could a mixing process involving a REE-rich cumulate such as the Hestnes nelsonite explain the high Zr and REE concentrations of the high-Zr jotunite? No. Indeed, if the jotunitic magma is not saturated in zircon and can thus dissolved up to 1.8 wt.% Zr at 1100°C following the calculation of Watson and Harrison (1983), the evolved jotunites are saturated in apatite at 1085°C (Table 1) and the primitive jotunite would assimilate 2 wt.% apatite to reach saturation at 1085°C with a maximum REE content 3 times lower than that of the primitive high-Zr jotunites.

In Fig. 10, the compositions of jotunites are compared with experimentally determined pairs of immiscible liquids (Charlier et al., 2013; Dixon and Rutherford, 1979) and with immiscible globules in the mesostasis of volcanic glasses (Philpotts, 1982). Out of all high-Zr samples, two rocks (samples #78-32-3 and #PM618) fit rather well the immiscibility fields and could be candidates for Fe-rich and Si-poor immiscible melts. Sample #78-32-3 is the 5-cm thick margin of the Tellnes dyke at Botnevatn. The rock is made up of the same minerals as the quartz mangerite #78-32 within the interior of the dyke, but in different proportions. The margin rock could thus represent a melt immiscible with the quartz mangeritic magma. This point is confirmed (within errors) when the partition coefficients of element E between iron-rich and silica-rich immiscible melts $D_E(L^M/L^F)$ at the nbo/t^F value of Si-rich melt are calculated following Bogaerts and Schmidt (2006) (Table 6).

It is noteworthy that the RAP LLD is continuous (Fig. 10) and that the Daly gap which is observed in most tholeiitic series (Charlier et al., 2013) between 50-55% SiO_2 and 60-65% SiO_2 is not observed. On the basis of the texture in quartz mangerite, such as in sample #78-32, we concur with Philpotts' interpretation (Philpotts, 1981) that immiscibility has taken place but the two liquids did not separate due to low viscosity contrast or to kinetic effects (Jakobsen et al., 2011; Veksler et al., 2006; 2007). We therefore suggest explaining the lack of Daly gap in the RAP LLD by this process. In the exceptional case of rock #78-32-3, some of the Fe-rich melt has effectively separated during the emplacement process to chill at the margin of the dyke.

ACCEPTED MANUSCRIPT

Now it remains to explain the origin of the other high-Zr jotunites and particularly of the most primitive ones that occur in the RAP as satellite dykes. Compared to experimental data and volcanic rocks (Fig. 10), immiscibility is not supported for Al_2O_3 and Na_2O contents that are too high. However, given that the available data on immiscibility concern only low pressure regime, immiscibility cannot be precluded at the higher pressure of anorthosite formation (up to 10-13 kbar) (Charlier et al., 2010a; and references therein). In the absence of any other possible explanation, we suggest that the high Zr and REE contents are hallmarks of immiscibility at higher pressure conditions than the pressure of emplacement (4-5 kbar) in anorthosite provinces.

Whereas the Si-rich melt conjugate with rock #78-32-2 (margin of the Tellnes dyke) approached a quartz mangeritic composition, the Si-rich melts associated with the primitive high-Zr jotunites are not known. It has been suggested that some quartz mangerite from the upper part of the BKSK intrusion could represent immiscible melts on top of the layered series (Wilson and Overgaard, 2005) despite objections raised by Duchesne et al. (1987) and Duchesne and Wilmart (1997). More work on trace element on apatite and zircon compositions in acidic rocks is needed to solve this issue.

5. Conclusions

Nelsonites are cumulates either in fractionated jotunitic melt (e.g. Kydlandsvatn deposit) or in a postulated immiscible Fe-rich melt (e.g. Hestnes deposit). Though the composition of the Fe-rich melt cannot be quantitatively determined by inversion from the cumulate mineral contents, because mineral/melt partition coefficient strongly depend on the structure of the Fe-rich melt and are not known, it can be qualitatively assessed that the Fe-rich melt is (1) rich in Fe, Ti and P; (2) enriched in incompatible elements (e.g. REE, Nb, Zr) concomitantly with compatible elements (e.g. Cr); (3) the REE distribution in the mafic melt shows a strong negative anomaly; and (4) the melt has high Zr/Hf and Nb/Ta ratios. There are pieces of evidence that the Hestnes deposit was formed in relatively more oxidizing conditions than the Kydlandsvatn deposit, conditions which could have favoured immiscibility.

In the most frequent conditions, the jotunite/ferrodiorite evolution does not yield immiscibility products and the normal liquid line of descent shows no Daly gap but a continuous evolution towards acidic rocks (mangerite/monzonite, quartz mangerite/quartz monzonite, charnockite/granite). Nevertheless, a rare rock type, high-Zr jotunite/ferrodiorite, which occurs in dykes, has characteristics in common with the Hestnes deposit (high REE

ACCEPTED MANUSCRIPT

contents and strong negative Eu anomaly, high Zr content and similar Sr-Nd isotope compositions). This suggests that high-Zr jotunites can be parent to the Hestnes nelsonite.

A high-Zr jotunite occurring as a contact rock in a quartz mangerite dyke is a good candidate to be a Fe-rich Si-poor immiscible melt. The absence of Daly gap in the jotunite LLD is explained by the poor separation of viscous immiscible melts, as earlier proposed by Philpotts (1981). Other high-Zr jotunites that occur in dykes cannot be explained neither by extreme fractionation of jotunite or ferrodiorite, nor by melting of adequate source rocks, nor by assimilation of cumulate nelsonite, nor by immiscibility at relatively low pressure. It is thus suggested that immiscibility at high pressure (in the 6-13 kbar range) is the only viable mechanism of formation, conditions that should be explored experimentally.

6. Acknowledgements

This work has greatly benefited from discussions and comments by O. Namur, B. Charlier and M. Higgins, and from a thorough review by J.K. Keiding. J. Scoates and K. Seifert are thanked for providing data on the LAC and AAP. E. Robinet is warmly thanked for her help in collecting some of the data.

7. Appendix: analytical methods

Whole rock major and trace elements

Whole-rock major elements analyses were performed by XRF on an ARL 9400 XP spectrometer on lithium tetra- and metaborate glass discs (FLUORE-X65®), with matrix corrections following the Traill-Lachance algorithm (ARL). Trace elements were analysed by ICP-MS on a VG Elemental Plasma Quad PQ2 after alkali fusion, following the method described in Vander Auwera et al. (1998a). Low Cr concentrations were analysed on an ARL Perform'X sequential spectrometer. FeO was measured by titration with $K_2Cr_2O_4$.

Mineral analysis

Fe-Ti oxide minerals and apatite were separated, after crushing and pulverizing, with a magnetic separator and heavy liquids. Fe-Ti oxide minerals were analysed for major and trace elements by XRF following Duchesne and Bologne (2009, 2011). Apatite was analysed for REE by ICP-MS on a VG Elemental Plasma Quad PQ2 using a calibration with standard samples determined by INAA (Roelandts and Duchesne, 1979).

Sr and Nd Isotopes

Sr and Nd isotopic compositions have been obtained at the Royal Museum for Central Africa on a GV Sector 54 multicollector thermo-ionisation mass spectrometer (TIMS) after chemical separation on ion exchange resins. The average $^{87}Sr/^{86}Sr$ ratio of the NBS SRM987 standard

ACCEPTED MANUSCRIPT

and $^{143}Nd/^{144}Nd$ ratio of the Rennes Nd standard during the period of analyses (one turret with 16 samples, including the present ones and 4 standards) were 0.710284 ± 0.000009 (2σ on 4 measurements) and 0.511954 ± 0.000004 (2σ on 4 measurements), respectively. Samples ratios have been standardized to a value of 0.710250 for NBS987 and to 0.511963 for the Rennes standard (corresponding to a La Jolla value of 0.511858).

8. References

Aleinikoff, J., Wright Horton Jr., J., Walter, M., 1996. Middle Proterozoic age for the Montpelier anorthosite, Goochland terrane, eastern Piedmont, Virginia. Geol. Soc. Amer. Bull.,108, 1481-1491.

Andersen, D.J., Lindsley, D.H., Davidson, P.M., 1993. QUILF: a Pascal program to assess equilibria among Fe-Mg-Ti oxides, pyroxenes, olivine, and quartz. Comput. Geosci. 19, 1333-1350.

Bogaerts, M., Schmidt, M., 2006. Experiments on silicate immiscibility in the system Fe_2SiO_4-$KAlSi_3O_8$-SiO_2-CaO-MgO-TiO_2-P_2O_5. Contrib. Mineral. Petrol. 152, 257-274.

Bolle, O., 1998. Mélanges magmatiques et tectonique gravitaire dans l'Apophyse de l'intrusion de Bjerkreim-Sokndal (Rogaland, Norvège): pétrologie, géochimie et fabrique magmatique, Geology. Liège University, Belgium.

Bolle, O., Duchesne, J.C., 2007. The apophysis of the Bjerkreim-Sokndal layered intrusion (Rogaland anorthosite province, SW Norway): a composite pluton build up by tectonically-driven emplacement of magmas along the margin of an AMC igneous complex. Lithos 98, 292-312.

Bolle, O., Demaiffe, D., Duchesne, J.C., 2003. Petrogenesis of jotunitic and acidic members of an AMC suite (Rogaland anorthosite province, SW Norway): a Sr and Nd isotopic assessment. Precamb. Res. 124, 185-214.

Bowen, N.L., 1928. The evolution of the igneous rocks. Princeton University Press, Princeton.

Cawthorn, R., 2013. Rare earth element abundances in apatite in the Bushveld Complex—A consequence of the trapped liquid shift effect. Geology 41, 603-606.

Cawthorn, R., 2014. Rare earth element abundances in apatite in the Bushveld Complex—A consequence of the trapped liquid shift. Geology 42, e319.

Charlier, B., Grove, T., 2012. Experiments on liquid immiscibility along tholeiitic liquid lines of descent. Contrib. Mineral. Petrol. 164, 27-44.

Charlier, B., Duchesne, J.C., Vander Auwera, J., 2006. Magma chamber processes in the Tellnes ilmenite deposit (Rogaland Anorthosite Province; SW Norway) and the formation of Fe-Ti ores in massif-type anorthosites. Chem. Geol. 234, 264-290.

Charlier, B., Namur, O., Grove, T., 2013. Compositional and kinetic controls on liquid immiscibility in ferrobasalt-rhyolite volcanic and plutonic series. Geochim. Cosmochim. Acta 113, 79-83.

Charlier, B., Vander Auwera, J., Duchesne, J.C., 2005. Geochemistry of cumulates from the Bjerkreim-Sokndal layered intrusion (S. Norway). Part II: REE and the trapped liquid fraction. Lithos 83, 255-276.

Charlier, B., Namur, O., Bolle, O., Latypov, R., Duchesne, J.-C., 2015. Fe-Ti-V-P ore deposits associated with Proterozoic massif-type anorthosites and related rocks. Earth-Sci. Rev. 141, 56-81.

ACCEPTED MANUSCRIPT

Charlier, B., Duchesne, J.C., Vander Auwera, J., Storme, J.-Y., Maquil, R., Longhi, J., 2010a. Polybaric fractional crystallization of high-alumina basalt parental magmas in the Egersund-Ogna massif-type anorthosite (Rogaland, SW Norway) constrained by plagioclase and high-alumina orthopyroxene megacrysts. J. Petrol. 51, 2547-2570.
Charlier, B., Sakoma, E., Sauvé, M., Stanaway, K., Vander Auwera, J., Duchesne, J.C., 2008. The Grader layered intrusion (Havre-Saint-Pierre anorthosite, Quebec) and genesis of nelsonite and other Fe-Ti-P ores. Lithos 101, 359-378.
Charlier, B., Namur, O., Duchesne, J.C., Wiszniewska, J., Parecki, A., Vander Auwera, J., 2009. Cumulate origin and polybaric crystallization of Fe-Ti oxide ores in the Suwalki anorthosite, Northeasten Poland. Econ. Geol. 104, 205-221.
Charlier, B., Namur, O., Malpas, S., De Marneffe, C., Duchesne, J.C., Vander Auwera, J., Bolle, O., 2010b. Origin of the giant Allard Lake ilmenite ore deposit (Canada) by fractional crystallization, multiple magma pulses and mixing. Lithos 117, 119-134.
Charlier, B., Namur, O., Toplis, M.J., Sciano, P., Cluzel, N., Higgins, M.D., Vander Auwera, J., 2011. Large-scale silicate liquid immiscibility during differentiation of tholeiitic basalt to granite and the origin of the Daly gap. Geology 39, 907-910.
Chen, W., Zhou, M.-F., Zhao, T.-P., 2013. Differentiation of nelsonitic magmas in the formation of the ~1.74 Ga Damiao Fe-Ti-P ore deposit, North China. Contrib. Mineral. Petrol. 165, 1341-1362.
Darling, R., Florence, F., 1995. Apatite light rare earth element chemistry of the Port Leyden nelsonite, Adirondac Highlands, New York: implications for the origin of nelsonite in anorthosite suite rocks. Economic Geology 90, 964-968.
Dixon, S., Rutherford, M., 1979. Plagiogranites as late-stage immiscible liquids in ophiolite and mid-ocean ridge suites. Earth Planet. Sci. Lett. 45, 45-60.
Duchesne, J.C., 1972. Iron-titanium oxide minerals in the Bjerkrem-Sogndal massif, South-Western Norway). J. Petrol. 13, 57-81.
Duchesne, J.C., 1978. Quantitative modeling of Sr, Ca, Rb and K in the Bjerkrem-Sogndal layered lopolith (S.W. Norway). Contrib. Mineral. Petrol. 66, 175-184.
Duchesne, J.C., 1996. Liquid ilmenite or liquidus ilmenite: a comment on the nature of ilmenite vein deposit, in: Demaiffe, D. (Ed.), Petrology and geochemistry of magmatic suites of rocks in the continental and oceanic crusts. ULB-MRAC, Bruxelles, pp. 73-82.
Duchesne, J.C., 1999. Fe-Ti deposits in Rogaland anorthosites (South Norway): geochemical characteristics and problems of interpretation. Mineral. Depos. 34, 182-198.
Duchesne, J.C., Bologne, G., 2009. XRF major and trace element determination in Fe-Ti oxide minerals. Geol. Belgica 12, 205-212.
Duchesne, J.-C., Bologne, G., 2011. Synthetic ilmenite as a blank to XRF trace element determination. Geol. Belgica 14, 103-106.
Duchesne, J.C., Charlier, B., 2005. Geochemistry of cumulates from the Bjerkreim-Sokndal layered intrusion (S. Norway). Part I: Constraints from major elements on the mechanism of cumulate formation and on the jotunite liquid line of descent. Lithos 83, 229-254.
Duchesne, J.C., Hertogen, J., 1988. Le magma parental du lopolithe de Bjerkreim-Sokndal (Norvège méridionale). C.R. Acad. Sci. Paris 306, 45-48.
Duchesne, J.C., Wilmart, E., 1997. Igneous charnockites and related rocks from the Bjerkreim-Sokndal layered intrusion (Southwest Norway): a jotunite (hypersthene monzodiorite)-derived A-type granitoid suite. J. Petrol. 38, 337-369.
Duchesne, J.C., Demaiffe, D., Roelandts, I., Weis, D., 1985a. Petrogenesis of monzonoritic dykes in the Egersund-Ogna anorthosite (Rogaland, S.W. Norway): trace elements and isotopic constraints. Contr. Mineral. Petrol. 90, 214-225.
Duchesne, J.C., Denoiseux, B., Hertogen, J., 1987. The norite-mangerite relationships in the Bjerkreim-Sokndal layered lopolith (SW Norway). Lithos 20, 1-17.

ACCEPTED MANUSCRIPT

Duchesne J.C., Liégeois J.P., Vander Auwera J. and Longhi J., 1999. The crustal tongue melting model and the origin of massive anorthosites. Terra Nova, 11, 100-105.
Duchesne, J.C., Maquil, R., Demaiffe, D., 1985b. The Rogaland anorthosites: facts and speculations, in: Tobi, A.C., Touret, J.L.R. (Eds.), The deep Proterozoic crust in the North Atlantic Province. Reidel, Doordrecht, pp. 449-476.
Duchesne, J.C., Wilmart, E., Demaiffe, D., Hertogen, J., 1989. Monzonorites from Rogaland (Southwest Norway): a series of rocks coeval but not comagmatic with massif-type anorthosites. Precamb. Res. 45, 111-128.
Dymek, R., Owens, B., 2001. Petrogenesis of apatite-rich rocks (Nelsonites and Oxide-apatite gabbronorites) associated with massif anorthosites. Econ. Geol. 96, 797-815.
Emslie, R.F., 1978. Anorthosite massifs, Rapakivi granites, and the late Proterozoic rifting of North America. Precamb. Res. 7, 61-98.
Force, E.R., 1991. Geology of titanium mineral deposits. Geol. Soc. Amer. Special Paper 259, 1-112.
Frost, B.R., Lindsley, D.H., 1992. Equilibria among Fe-Ti oxides, pyroxenes, olivine, and quartz: Part II. Application. Amer. J. Science 77, 1004-1020.
Frost, B.R., Lindsley, D.H., Andersen, D.J., 1988. Fe-Ti oxide-silicate equilibria: Assemblages with fayalitic olivine. Amer. Mineral. 73, 727-740.
Green, T., 1994. Experimental studies of trace element partitioning applicable to igneous petrogenesis -Sedona 16 years later. Chem. Geol. 117, 1-36.
Harrison, T.M., Watson, E.B., 1984. The behavior of apatite during crustal anatexis: equilibrium and kinetic considerations. Geochim. Cosmochim. Acta 48, 1467-1477.
Hubaux, A., 1960. Les gisements de fer titané de la région d'Egersund (Norvège). N. Jb. Miner. Festband Ramdohr 94, 926-992.
Irvine, T.N., 1982. Terminology of layered intrusions. J. Petrol. 23, 127-162.
Jakobsen, J.K., Veksler, I., Tegner, C., Brooks, C., 2005. Immiscible iron- and silica-rich melts in basalt petrogenesis documented in the Skaergaard intrusion. Geology 33, 885-888.
Jakobsen, J.K., Veksler, I., Tegner, C., Brooks, C., 2011. Crystallization of the Skaergaard intrusion from an emulsion of immiscible iron- and silica-rich liquids: evidence from melt inclusions in plagioclase. J. Petrol. 52, 345-353.
Jensen, J.C., Nielsen, F.M., Duchesne, J.C., Demaiffe, D., Wilson, J.R., 1993. Magma influx and mixing in the Bjerkreim-Sokndal layered intrusion, South Norway: evidence from the boundary between two megacyclic units at Storeknuten. Lithos 29, 311-325.
Kelsey, D.E., Hand, M., 2014. On ultrahigh temperature crustal metamorphism: Phase equilibria, trace element thermometry, bulk composition, heat sources, timescales and tectonic settings. Geosci. Front., 6, 1-46.
Kolker, A., 1982. Mineralogy and geochemistry of Fe-Ti oxide and apatite (nelsonite) deposits and evaluation of liquid immiscibility hypothesis. Econ. Geol. 77, 114-1158.
Kozlowski, A., Wiszniewska, J., 2001. The nelsonite problem: the origin by melt immiscibility, in: Korneliussen, A. (Ed.), GEODE field trip workshop on ilmenite deposits in the Rogaland anorthosite province, S. Norway. NGU Report no. 2001.042.
Lattard, D., Sauerzapf, U., Käseman, M., 2005. New calibration data for the Fe-Ti oxide thermo-oxybarometers from experiments in the Fe-Ti-O system at 1 bar, 1000-1300°C and a large range of oxygen fugacities. Contrib. Miner. Petrol. 149, 735-754.
Lindsley, D.H., 2003. Do Fe-Ti oxide magmas exist? Geology: Yes; Experiments: No! NGU Special Public. 9, 34.
Longhi, J., 2005. A mantle or mafic crustal source for Proterozoic anorthosites? Lithos 83, 183-198.

ACCEPTED MANUSCRIPT

Longhi, J., Vander Auwera, J., Fram, M., Duchesne, J.C., 1999. Some phase equilibrium constraints on the origin of Proterozoic (Massif) anorthosites and related rocks. J. Petrol. 40, 339-362.
Maquil, R., Duchesne, J.C., 1984. Géothermométrie par les pyroxènes et mise en place du massif anorthositique d'Egersund-Ogna (Rogaland, Norvège méridionale). Ann. Soc. Géol. Belg. 107, 27-49.
Michot, P., 1960. La géologie de la catazone: le problème des anorthosites, la palingenèse basique et la tectonique catazonale dans le rogaland méridional (Norvège méridionale). Norges geol. undersök. 212g, 1-54.
Mitchell, J.N., Scoates, J.S., Frost, C.D., Kolker, A., 1996. The geochemical evolution o anorthosite residual magmas in the Laramie Anorthosite Complex, Wyoming. J. Petrology 37, 637-660.
Naldrett, A.J., 2004. Magmatic sulfide deposits: geology, geochemistry and exploration. Springer, Berlin, Heidelberg, New York.
Namur, O., Charlier, B., Holnes, M., 2012. Dual origin of Fe-Ti gabbros by immiscibility and fractional crystallization of eveolved tholeiitic basalts in the Sept Iles layered intrusion. Lithos 154, 100-114.
Namur, O., Charlier, B., Toplis, M.J., Higgins, M.D., Liégeois, J.-P., Vander Auwera, J., 2010. Crystallization sequence and magma chamber processes in the ferrobasaltic Sept Iles layered intrusion, Canada. J. Petrol 51, 1203-1236.
Nasipuri, P., Bhattacharya, A., Satyanarayanan, M., 2011. Localized pluton deformation and linked focused flow of low volume fraction residual melt in deforming plagioclase cumulates. Geol. Soc. Amer. Bull.123, 669-680.
Naslund, H., 1983. The effect of oxygen fugacity on liquid immiscibility in iron-bearing silicate melts. Am.J. Sci. 283, 1034-1059.
Philpotts, A.R., 1967. Origin of certain iron-titanium oxide and apatite rocks. Econ. Geol. 62, 303-315.
Philpotts, A.R., 1981. A model for the generation of massif-type anorthosites. Can. Mineral. 19, 233-253.
Philpotts, A.R., 1982. Compositions of immiscible liquids in volcanic rocks. Contrib. Mineral. Petrol. 80, 201-218.
Robins, B., Tumyr, O., Tysseland, M., Garmann, L.B., 1997. The Bjerkreim-Sokndal Layered Intrusion, Rogaland, S.W. Norway: Evidence from marginal rocks for a jotunite parent magma. Lithos 39, 121-133.
Roelandts, I., Duchesne, J.C., 1979. Rare-earth elements in apatite from layered norites and iron-titanium oxide ore-bodies related to anorthosites (Rogaland, S.W. Norway), in: Ahrens, L.H. (Ed.), Origin and distribution of the elements. Pergamon, pp. 199-212.
Ryerson, F.J., Hess, P.C., 1978. Implications of liquid-liquid distribution coefficients to mineral-liquid partitioning. Geochim. Cosmochim. Acta 42, 921-932.
Sajeev, K., Osanai, Y., 2004. Ultrahigh-temperature metamorphism (1150 °C, 12 kbar) and multistage evolution of Mg-, Al-rich granulites from the central Highland Complex, Sri Lanka. J. Petrol. 45, 1821-844.
Schärer, U., Wilmart, E., Duchesne, J.C., 1996. The short duration and anorogenic character of anorthosite magmatism: U-Pb dating of the Rogaland complex, Norway. Earth Planet. Sci. Lett. 139, 335-350.
Schiellerup, H., Korneliussen, A., Heldal, T., Marker, M., Bjerkgård, T., Nilsson, L.-P., 2003. Mineral resources in the Rogaland Anorthosite Province, South Norway, in: Duchesne, J.C., Korneliussen, A. (Eds.), Ilmenite deposits and their geological environment. NGU Special Publication 9, pp. 117-135.

ACCEPTED MANUSCRIPT

Schmidt, M., Connoly, J., Günther, D., Bogaerts, M., 2006. Element partitioning: the role of melt structure. Science 312, 1646-1650.
Scoates, J.S., Chamberlain, K.R., 2003. Geochronology, geochemical and isotopic constraints on the origin of monzonitic and related rocks in the Laramie anorthosite complex, Wyoming, USA. Precamb. Res. 124, 269-304.
Scoates, J.S., Frost, C.D., Mitchell, J.N., Lindsley, D.H., Frost, B.R., 1996. Residual-liquid origin for a monzonoritic intrusion in a mid-Proterozoic anorthosite complex: The Sybille intrusion, Laramie anorthosite complex, Wyoming. Geol. Soc. Amer. Bull. 108, 1357-1371.
Seifert, K.E., Dymek, R., Whitney, P., Haskin, L., 2010. Geochemistry of massif anorthosite and associated rocks, Adirondack Mountains, New York. Geosphere 6, 855-899.
Snyder, D., Carmichael, I.S.E., Wiebe, R.A., 1993. Experimental study of liquid evolution in a Fe-rich, layered mafic intrusion: constraints of Fe-Ti oxide precipitation on the T-fO2 and T-ro path of tholeiitic magmas. Contrib. Mineral. Petrol. 113, 73-86.
Spencer, K.J., Lindsley, D.H., 1966. A solution model for coexisting iron-titanium oxides. Amer. Mineral. 66, 1189-1201.
Sun, S.S., McDonough, W.F., 1989. Chemical and isotopic systematices of oceanic basalts: implications for mantle composition and processes, in: Saunders, A.D., Norry, M.J. (Eds.), Magmatism in Ocean Basins. Geological Society of London Special Publication, pp. 313-345.
Tegner, C., Cawthorn, R., Kruger, F., 2006. Cyclicity in the main and upper zones of the Bushveld Complex, South Africa: Crystallization from a zoned magma sheet. J. Petrol. 47, 2257-2279.
Tollari, N., Barnes, S.-J., Cox, R., Nabil, H., 2008. Trace element concentrations in apatites from the Sept-ïles intrusive suite, Canada - Implications for the genesis of nelsonites. Chem. Geol. 252, 180-190.
Toplis, M., Carroll, M.R., 1995. An experimental study of the influence of oxygen fugacity on Fe-Ti oxide stability, phase relations, and mineral-melt equilibria in ferro-basaltic systems. J. Petrol. 36, 1137-1170.
Van Tongeren, J., Mathez, E., 2012. Large-scale liquid immiscibility at the top of the Bushveld Complex, South Africa. Geology 40, 491-494.
Van Tongeren, J., Mathez, E., 2014. Rare earth element abundances in apatite in the Bushveld Complex— A consequence of the trapped liquid shift effect. Comment. Geology 42, e318.
Vander Auwera, J., Bologne, G., Roelandts, I., Duchesne, J.C., 1998a. Inductively coupled plasma-mass spectrometry (ICP-MS) analysis of silicate rocks and minerals. Geol. Belgica 1, 49-53.
Vander Auwera, J., Longhi, J., 1994. Experimental study of a jotunite (hypersthene monzodiorite): constraints on the parent magma composition and crystallization conditions (P, T, fO2) of the Bjerkreim-Sokndal layered intrusion. Contrib. Mineral. Petrol.118, 60-78.
Vander Auwera, J., Longhi, J., Duchesne, J.C., 1998b. A liquid line of descent of the jotunite (hypersthene monzodiorite) suite. J. Petrol. 39, 439-468.
Vander Auwera, J., Weis, D., Duchesne, J.C., 2006. Marginal mafic intrusions as indicators of dowslope draining of dense residual melts in anorthosite diapirs? Lithos 89, 329-352.
Veksler, I., Charlier, B., 2015. Silicate liquid immiscibility in layered intrusions, in: Charlier, B., Namur, O., Latypov, R., Tegner, C. (Eds.), Layered intrusions. Springer Geology, Dordrecht, p. 229-258.
Veksler, I., Dorfman, A., Borisov, A., Wirth, R., Dingwell, D., 2007. Liquid immiscibility and the evolution of basaltic magma. J. Petrol. 48, 2187-2210.
Veksler, I., Dorfman, A., Danyushevsky, L., Jakobsen, J., Dingwell, D., 2006. Immiscible silicate liquid partition coefficients: implications for crystal-melt element partitioning and basalt petrogenesis. Contrib. Mineral. Petrol. 152, 685-702.

ACCEPTED MANUSCRIPT

Vicenzi, E., Green, T., Sie, S., 1994. Effect of oxygen fugacity on trace-element partitioning between immiscible silicate melts at atmospheric pressure: a proton and electron microprobe study. Chem. Geol. 117, 355-360.
Wang, C.Y., Zhou, M.-Y., 2013. New textural and mineralogical constraints on the origin of the Hongge Fe-Ti-V oxide deposit, SW China. Mineral. Depos. 48, 787-798.
Watson, E.B., 1976. Two-liquid partition coefficients: experimental data and geochemical significance. Contrib. Mineral. Petrol. 56, 119-134.
Watson, E.B., Harrison, T.M., 1983. Zircon saturation revisited: temperature and compositional effects in a variety of crustal magma types. Earth Planet. Sci. Lett. 64, 295-304.
Wilmart, E., 1988. Etude géochimique des charnockites du Rogaland. Mém. Sc. Terre Univ. Curie, Paris 88-20.
Wilmart, E., Demaiffe, D., Duchesne, J.C., 1989. Geochemical constraints on the genesis of the Tellnes ilmenite deposit (S.W. Norway). Econ. Geol. 84, 1047-1056.
Wilson, J.R., Overgaard, G., 2005. Relationships between the Layered series and the overlying evolved rocks in the Bjerkreim-Sokndal Intrusion, southern Norway. Lithos 83, 277-298.
Wilson, J.R., Robins, B., Nielsen, F., Duchesne, J.C., Vander Auwera, J., 1996. The Bjerkreim-Sokndal layered intrusion, Southwest Norway, in: Cawthorn, R.G. (Ed.), Layered Intrusions. Elsevier, Amsterdam, pp. 231-256.
Zhou, M.-F., Chen, W.T., Wang, C.Y., Prevec, S.A., Liu, P.P., Howarth, G.H., 2013. Two stages of immiscible liquid seperation in the formation of Panzhihua-type Fe-Ti-V oxide deposits, SW China. Geosci. Front. 4, 481-502.

ACCEPTED MANUSCRIPT

ACCEPTED MANUSCRIPT

Conflict of interest

I declare that this paper does not rise any conflict of interest.

JC Duchesne

ACCEPTED MANUSCRIPT

ACCEPTED MANUSCRIPT

Duchesne & Liégeois

Table captions

Table 1: Composition of RAP main type of jotunites, of the quartz mangerite dyke at Botnevatn and of high-Zr jotunites/ferrodiorites in the RAP, LAC and AAP. Data from the literature except for sample #76.27.

Table 2: Major (wt.%) and trace element (ppm) compositions of ores from the Kydlandsvatn and Hestnes ore bodies.

Table 3: Composition of Fe-Ti oxide minerals in selected samples of Kydlandsvatn and Hestnes deposits

Table 4: REE compositions (ppm) in apatite from the Kydlandsvatn and Hestnes nelsonites.

Table 5: Rb-Sr and Sm-Nd isotopic compositions of apatites from Rogaland Fe-Ti deposits.

Table 6: Comparison of the chilled jotunite #78-32-3 with the range of compositions of its conjugate immiscible melt (quartz mangerite #78-32) calculated with the melt-melt partition coefficients for Si, Ti, Fe, Ca, K and P of Bogaerts & Schmidt (2006)

.

Figure captions

Fig. 1. Geological sketch map of the Rogaland Anorthosite Province (RAP) (after Bolle and Duchesne, 2007). Abbreviations: EGOG: Egersund-Ogna massif; He: Helleren anorthosite massif; Hå: Håland anorthosite massif; ÅS: Åna-Sira anorthosite massif; BKSK: Bjerkreim-Sokndal layered intrusion. Numbers refer to jotunitic dyke samples from the Vettaland and Tellnes dykes studied here.

Fig. 2. Geological map of the Norito-charnockitic Zone (modified after Hubaux, 1960). Abbreviations: EGOG: Egersund-Ogna massif; He: Helleren anorthosite massif; Hå: Håland anorthosite massif; E: Egersund deposit; H: Hestnes deposit; R: Rødemyr lens; Kaknuden

ACCEPTED MANUSCRIPT

deposit; Ky: Kydlandsvatn deposit. Number 76-27 refers to the Løyning jotunitic dyke sample studied here. For clarity, the dolerite dyke system is not represented.

Fig. 3. Characteristic features of the Kydlandsvatn deposit. A: Layers of ilmenite ore interleaved with anorthosite and norite layers. B: Microphoto under reflected light. Hemo-ilmenite (hemo-ilm) is associated with magnetite (mag) with minute spinel exsolutions, apatite (ap) and spinel (spi). Arrow shows a baddeleyite (bd) grain close to an exsolution. Ilmenite-spinel reaction rims at the contact between hemo-ilmenite and magnetite as well as a decrease in hematite exsolutions towards the contact are observed. Spinel grains also straddle the contact between magnetites (sample #79-19-1b).

Fig. 4. Characteristic features of the Hestnes deposit. A: Nelsonite layer associated with a coarse-grained magnetite layer. Arrow n°1 indicates a magnetite phenoblast ("platy" magnetite). Arrow n°2: Sulphide crystals. In the magnetite layer, note the mosaic structure of magnetite grains with 120° junctions (sample #79-19-2; polished section). B: Photo of a 10 mm-long zircon crystal in the quartz diorite close to the contact with the country rock (sample #00-50). C: Zircon crystal interstitial to apatite and Fe-Ti oxide minerals (transmitted light) (sample #00-41). D. Mosaic of Ti-magnetite grains with two generations of spinel exsolutions, ilmenite and apatite grains (sample #66-33, reflected light). The layering plane is indicated by a dashed line. Abbreviations: Ti-mag: Ti-magnetite, Ilm: ilmenite, Ap: apatite.

Fig. 5. Various correlations between trace and major elements in whole-rocks and apatite compositions from the Kydlandsvatn and Hestnes deposits. Data from Tables 2 and 4.

Fig. 6. Chondrite-normalized REE compositions of apatite from Kydlandsvatn and Hestnes nelsonites (data from Table 4) compared to previous analyses (shaded areas) (Duchesne, 1999). Apatite compositions from the BKSK layered intrusion are shown by dashed lines: the lowest composition is from MCU3 (gabbro-norites), the intermediate one from le low part of MCU4, and the highest from the upper part of MCU4 (jotunites) (Roelandts and Duchesne, 1979). Normalizing values from Sun and McDonough (1989).

Fig. 7. ε_{Nd} vs $^{87}Sr/^{86}Sr$ ratios at 930 Ma in representative samples of jotunites, acidic rocks and apatite from various Fe-Ti deposits. Mixing hyperbolae linking crustal end-members to

ACCEPTED MANUSCRIPT

the most primitive jotunite are shown with 10% ticks. Data in Table 5 and from Bolle et al. (2003).

Fig. 8. Major element contents vs Mg# of Zr-rich ferrodiorites from the RAP, LAC and AAP compared to the RAP liquid line of descent (data from Table 1 and from Vander Auwera et al., 1998b).

Fig. 9. Selected trace elements concentrations (ppm) and ratios vs Mg# (= mol. MgO/MgO+FeOt) of Zr-rich ferrodiorites from the LAC, RAP and AAP compared to the RAP LLD (data from Table 1 and from Vander Auwera et al., 1998b).

Fig. 10. Harker diagrams of Zr-rich ferrodiorites from the RAP and LAC (data in Table 1) compared to immiscible globules in the mesostasis of volcanic glasses (Philpotts, 1982) (shaded domains) and to experimentally produced immiscible pairs of Charlier and Grove (2012) (domains enclosed by dashed lines).

ACCEPTED MANUSCRIPT

ACCEPTED MANUSCRIPT

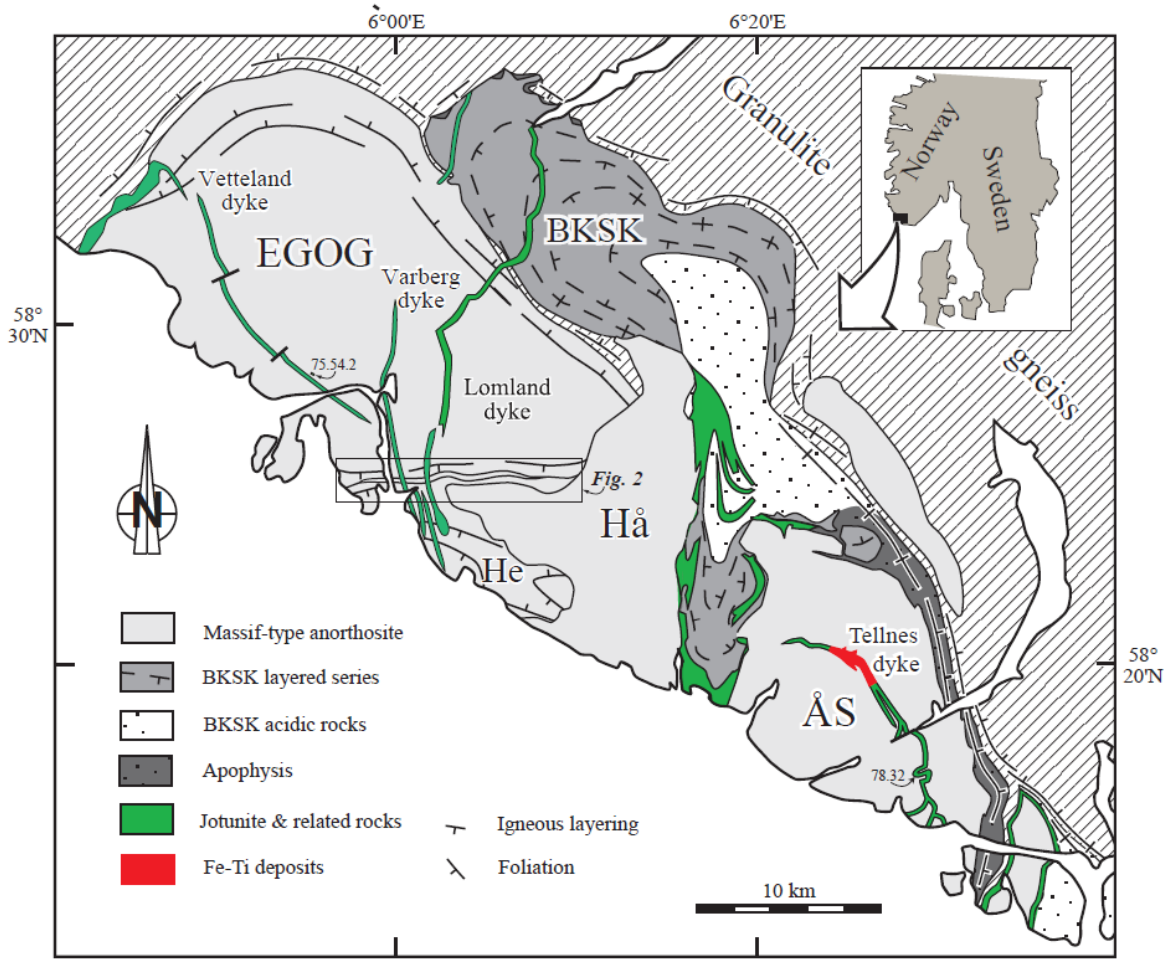

Fig. 1

ACCEPTED

ACCEPTED MANUSCRIPT

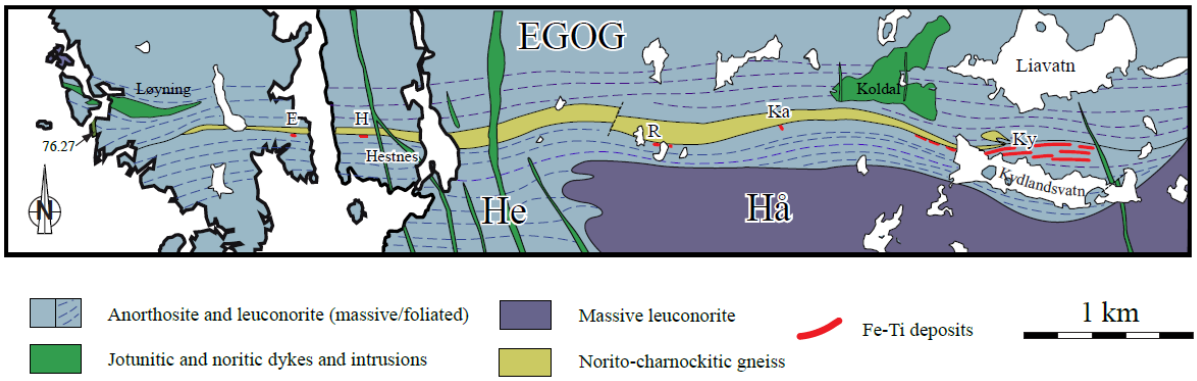

Fig. 2

ACCEPTED MANUSCRIPT

ACCEPTED MANUSCRIPT

Fig. 3

ACCEPTED MANUSCRIPT

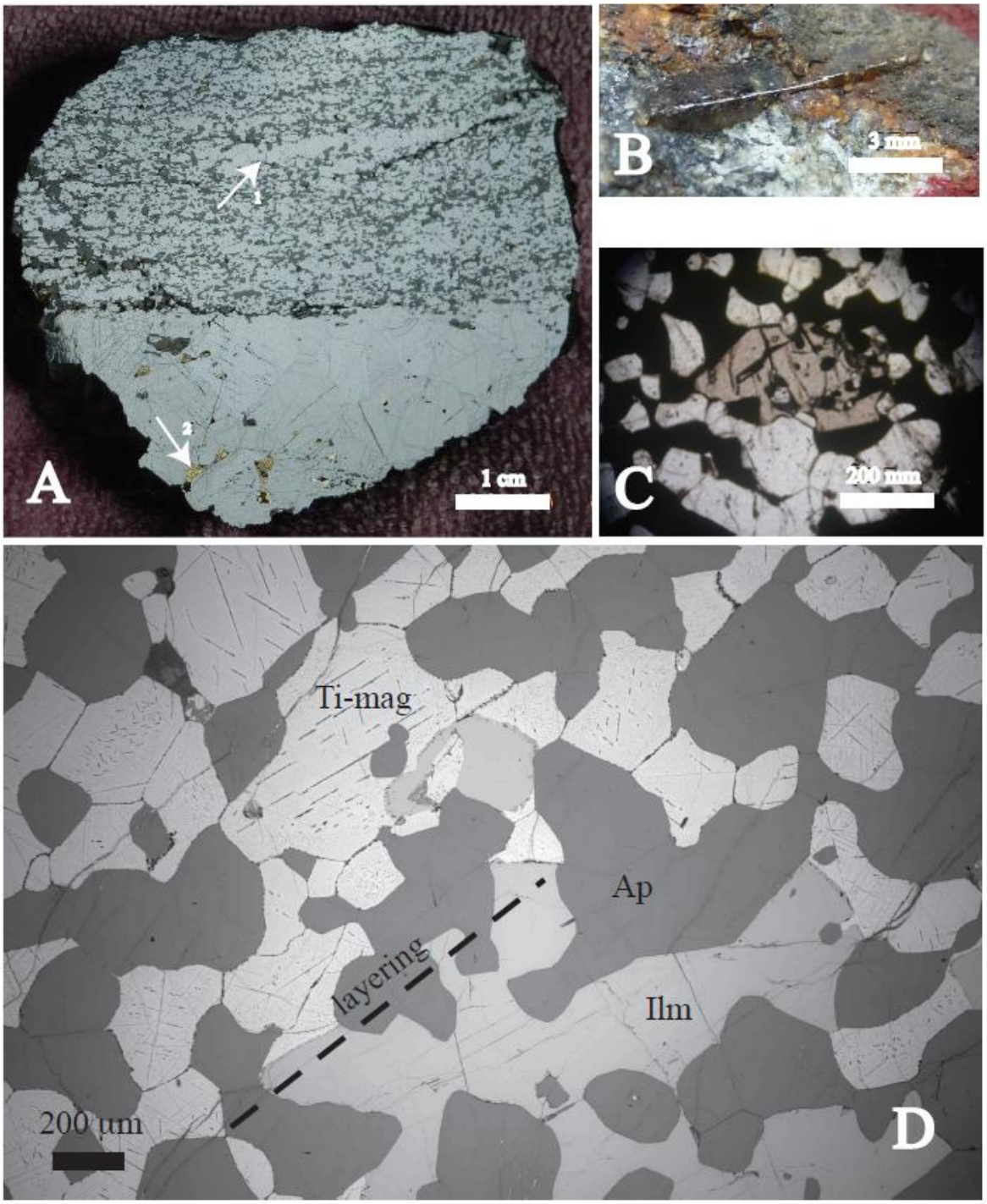

Fig. 4

ACCEPTED MANUSCRIPT

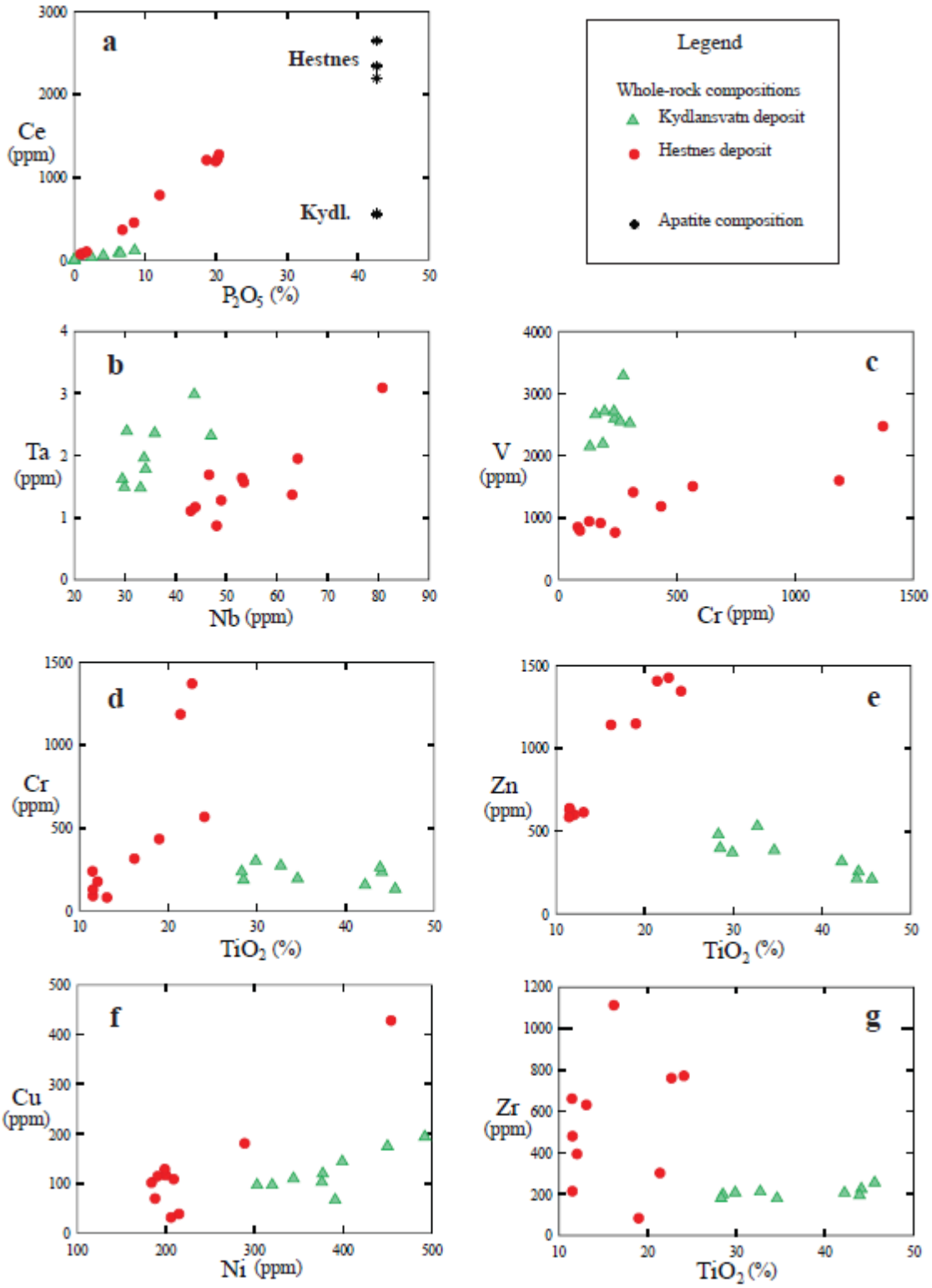

Fig. 5

ACCEPTED MANUSCRIPT

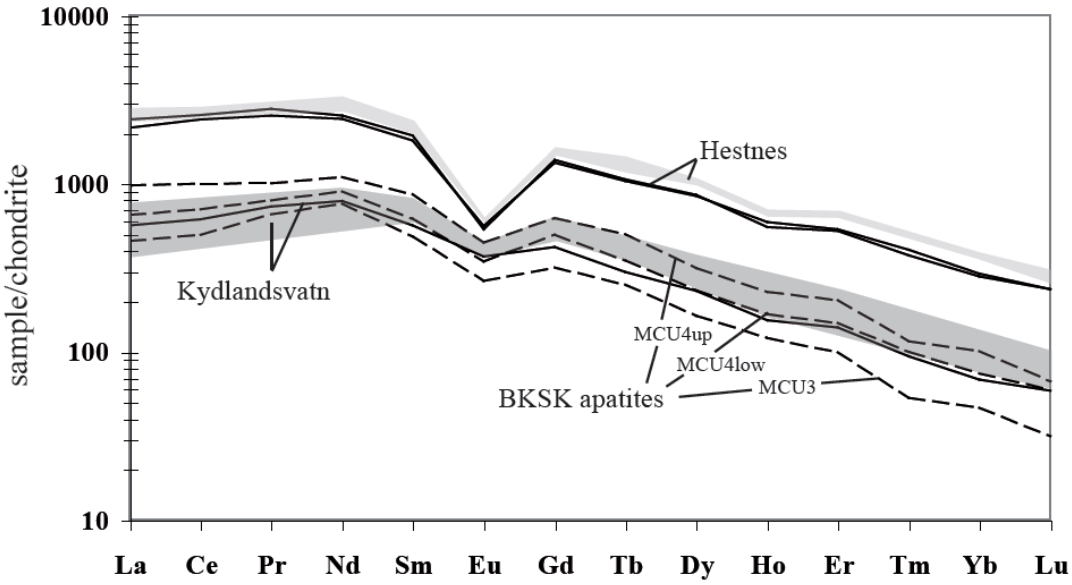

Fig. 6

ACCEPTED MA

ACCEPTED MANUSCRIPT

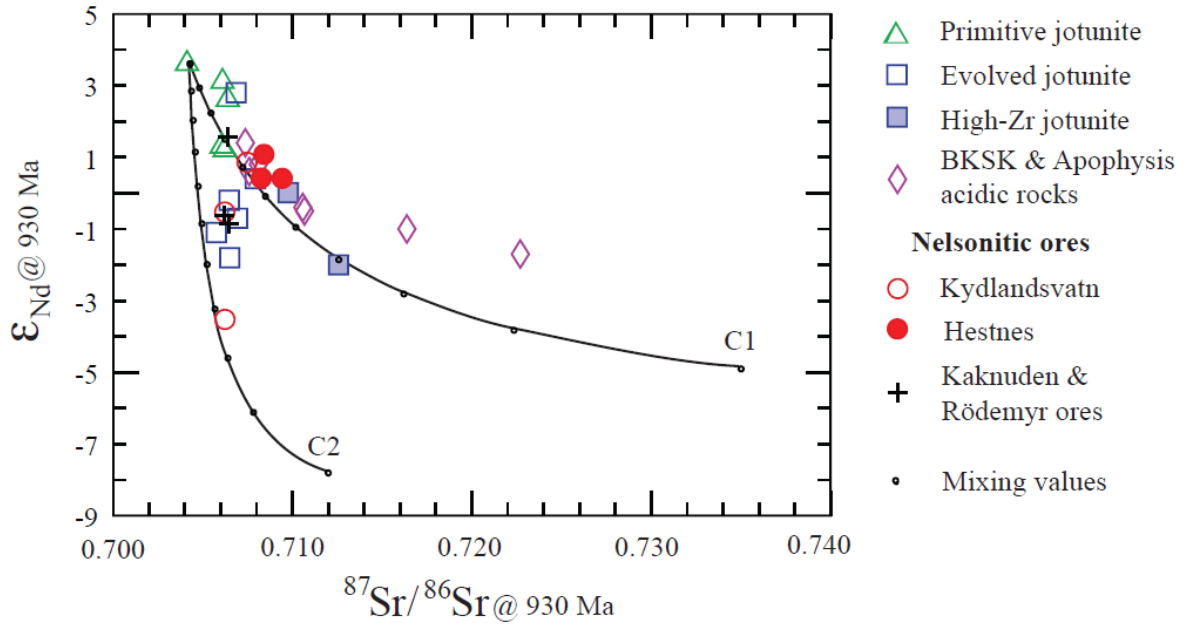

Fig. 7

ACCEPTED MANUSCRIPT

ACCEPTED MANUSCRIPT

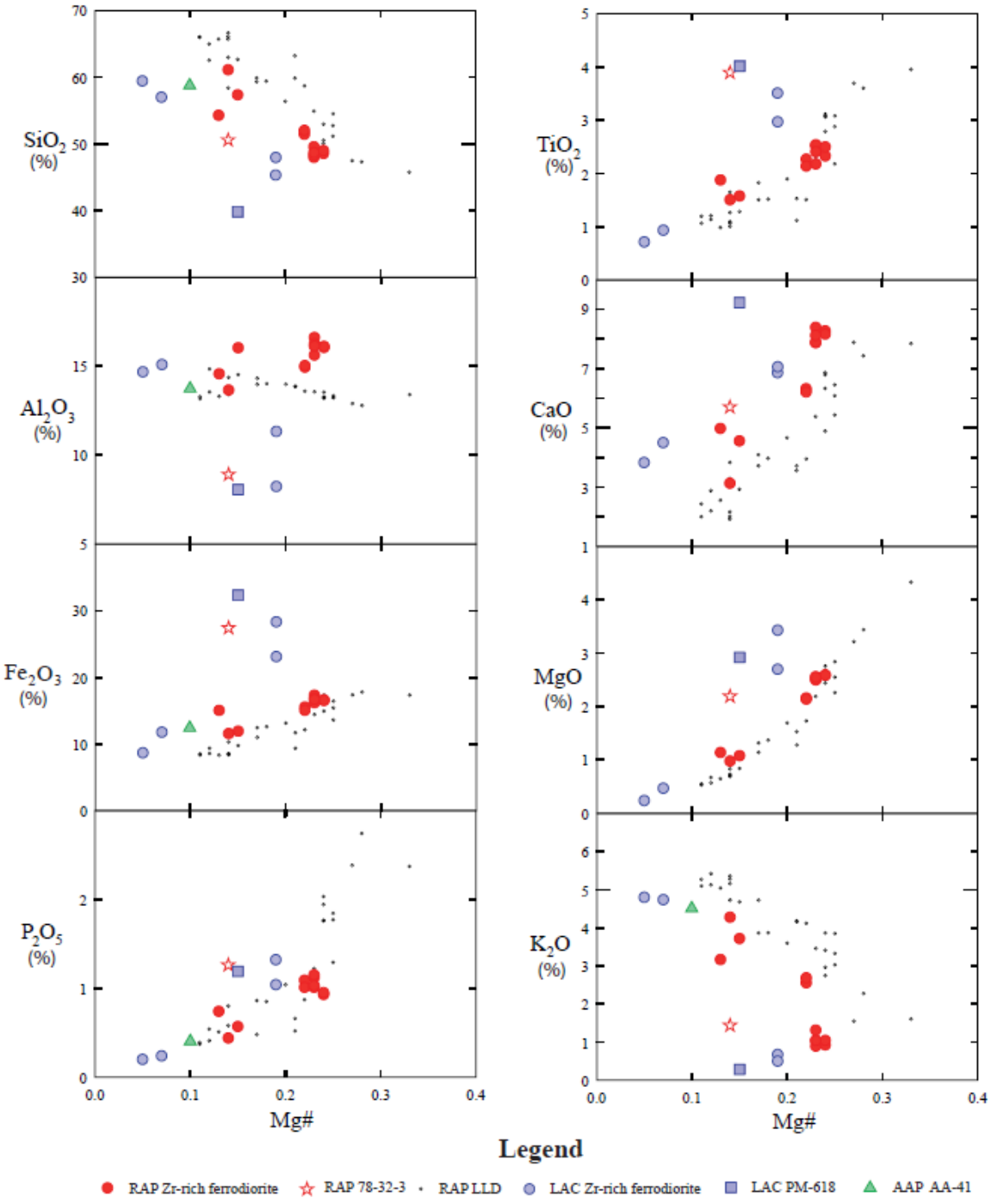

Fig. 8

ACCEPTED MANUSCRIPT

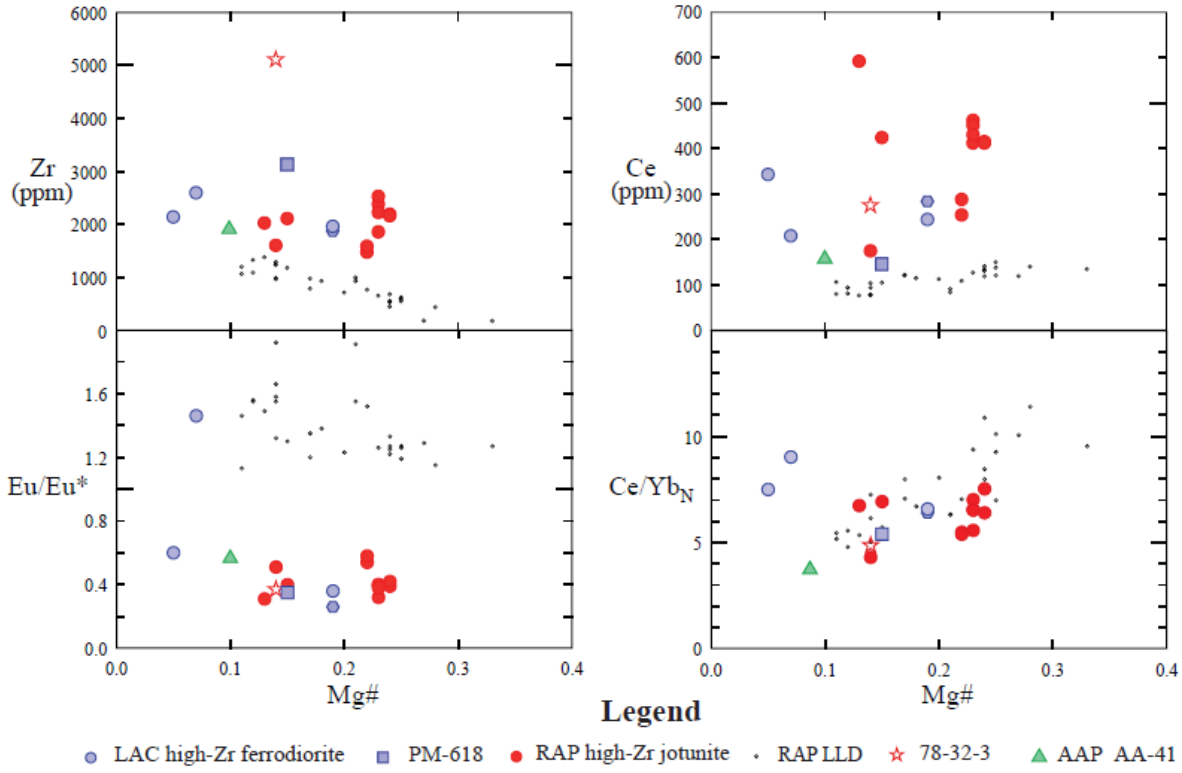

Fig. 9

ACCEPTED

ACCEPTED MANUSCRIPT

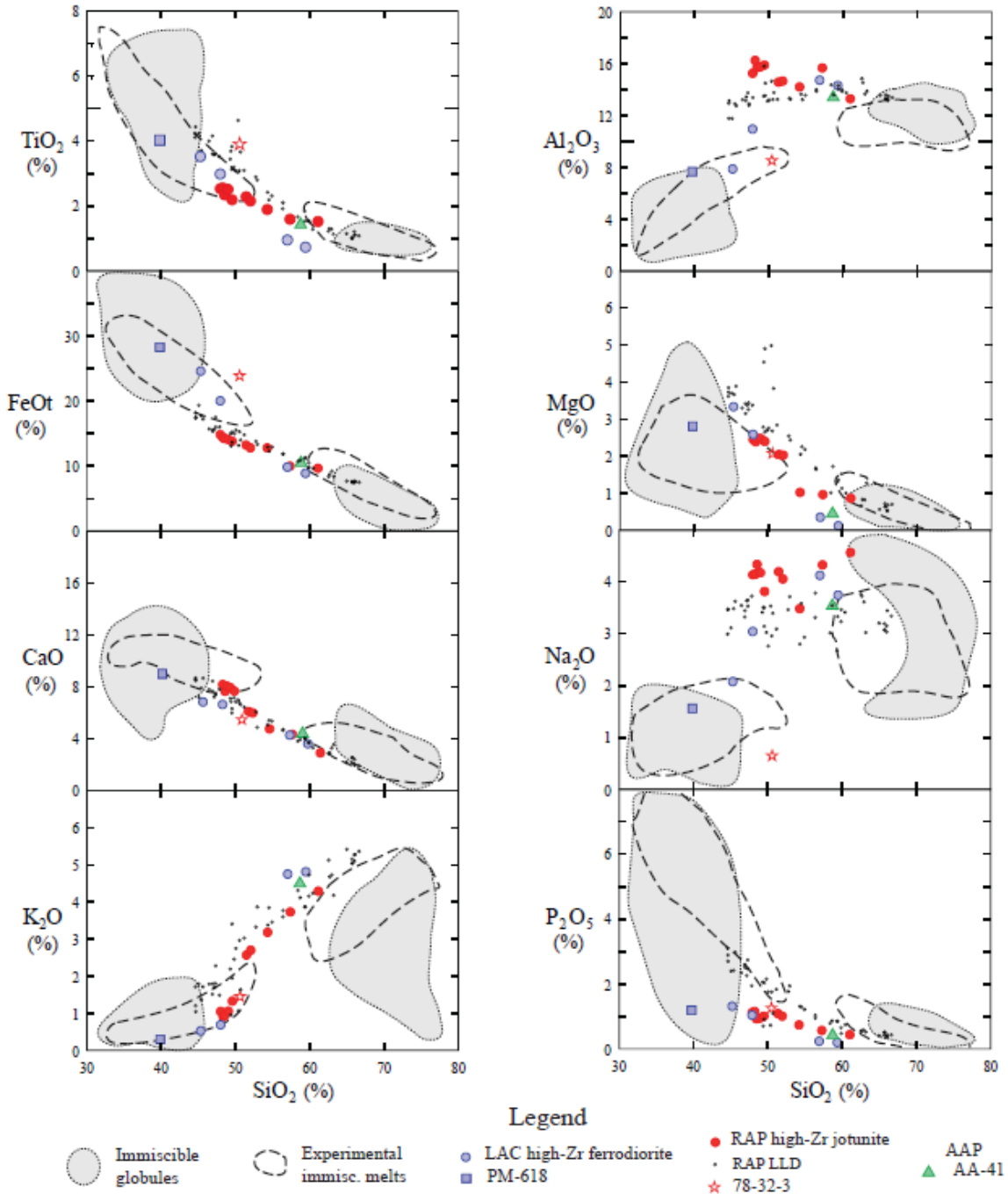

Fig. 10

ACCEPTED MANUSCRIPT

Table 1 Composition of RAP main type of jotunites, of the quartz mangerite dyke at Botnevatn and of high-Zr ferrodiorites/jotunites in the RAP, LAC and AAP. Data from the literature except for sample #76.27

	High-Zr jotunite																		
	RAP			**RAP**										**LAC**					**AAP**
	Average jotunites		**Botnevatn**	**Satellite of Telness dyke**					**Satellite of Apophysis**			**Sirevåg**	**Loyning**	**Botnevatn**	**SCc** (a)		**PMa** (b)	**RMP** (c)		**Lake Placid**
	Primitive	Evolved	**78.32**	**T13**	**84.2**	**T11**	**T12**	**T20-1**	**93BN56**	**93BN61**	**93BN50**	**75.54.2**	**76.27**	**78.32.3**	**BM-21**	**BM-22**	**PM-618**	**PM436**	**MPK60a**	**AA-41**
Major elements (wt%)																				
SiO_2	49.65	48.28	65.71	47.98	48.32	48.55	49.00	49.56	54.29	57.35	61.12	52.02	51.45	50.58	45.37	47.97	39.85	59.44	57.00	58.79
TiO_2	4.23	3.45	0.99	2.52	2.54	2.33	2.50	2.18	1.88	1.58	1.51	2.14	2.27	3.89	3.51	2.97	4.01	0.72	0.94	1.41
Al_2O_3	14.14	13.32	13.31	15.63	16.62	16.06	16.12	16.26	14.58	16.04	13.67	15.04	14.95	8.92	8.26	11.34	8.07	14.69	15.1	13.76
Fe_2O_{3t}	15.52	17.20	8.37	17.34	16.85	16.66	16.54	16.21	15.07	11.96	11.59	15.08	15.57	27.42	28.33	23.13	32.3	8.70	11.8	12.42
MnO	0.16	0.23	0.11	0.15	0.28	0.24	0.28	0.18	0.24	0.18	0.18	0.23	0.25	0.34	0.47	0.35	0.56	0.24	0.26	0.21
MgO	4.87	3.11	0.65	2.56	2.50	2.59	2.59	2.51	1.14	1.08	0.98	2.14	2.16	2.19	3.43	2.7	2.92	0.24	0.47	0.59
CaO	6.68	7.34	2.56	8.39	7.87	8.27	8.16	7.89	4.98	4.56	3.13	6.21	6.32	5.70	7.07	6.86	9.22	3.83	4.5	4.54
Na_2O	3.52	3.39	3.07	4.13	4.14	4.33	4.17	3.81	3.48	4.32	4.56	4.05	4.19	0.65	2.09	3.04	1.56	3.74	4.12	3.54
K_2O	1.38	2.25	5.04	1.04	0.90	0.93	1.05	1.32	3.17	3.72	4.28	2.69	2.56	1.44	0.51	0.68	0.29	4.8	4.74	4.51
P_2O_5	1.01	2.23	0.51	1.12	1.15	0.93	0.95	1.01	0.74	0.57	0.44	1.01	1.09	1.26	1.32	1.04	1.19	0.2	0.24	0.40
Total	100.09	100.14	99.76	99.88	100.14	99.94	100.38	100.11	98.69	100.51	100.59	99.55	100.81	100.71	100.29	100.08	99.97	97.575	99.17	100.16
Mg#	0.38	0.26	0.13	0.23	0.23	0.24	0.24	0.23	0.13	0.15	0.14	0.22	0.22	0.14	0.19	0.19	0.15	0.05	0.07	0.10
Trace elements																				

ACCEPTED MANUSCRIPT

(ppm)																			
U	1.31	0.31	0.20	0.59	0.76	0.46	0.42	0.62	2.04	1.30	1.44	0.53	0.791	0.50					
Th	2.75	0.68	0.66	3.00	2.69	2.57	3.29	5.00	15.00	7.15	2.48	2.11	2.748	1.37					2.01
Th/U	2.9	2.9	3.3	5.1	3.5	5.6	7.8	8.1	7.4	5.5	1.7	4.0	3.5	2.7					
Zr	198	444	1387	23 84	186 3	21 97	216 6	253 3	2030	2114	1609	1591	1480	5110	1880	1967	3135	2143	2600	1904
Hf	5.3	9.4	33	57	57	54	52	58	57	49	45	39	25	124						44
Zr/Hf	37	47	43	42	33	41	41	44	36	43	36	40	59	41						43
Nb	22	29	18	39	26	35	46	28	50	52	52		41	73						39
Ta	1.1	1.6	0.9	1.3	0.9	1.2	1.6	0.9	1.7	1.7	2.3	1.9	1.9	3.4						2.2
Nb/Ta	21	18	19	30	28	29	30	33	29	31	22		21	22						18
Rb	22	17	71	4.6	2.7	3.9	3.7	7.8	67	72	80	42	37	11	4.7		2.0	143	72	83
Sr	439	394	128	49 4	532	45 3	494	476	257	287	149	347	304	82	171	242	179	157	276	247
Ba	611	1392	1482	48 8	562	46 6	507	883	1382	1682	1106	1613	1400	393	425	269	395	1282	3400	1171
Sc	20	27	16	35	34	33	33	31				28		52	55	47	63	29		
Ni	44	13	*<25*	16	52	26	11	9	<25	<25	<25	<10	14	10	21	10	36	7		8
V	257	136	72	81	157	88	70	72	55	54	32	66	79		112	90	86	144		
Cr	19	46	6	17	22	19	28	19	<25	<25	<25	17	13	20	17	14	22			7
Co	52	41	7	20	27	23	20	21	15	14	12	21	25	24						
Zn	137	219	151	25 3	280	34 2	225	279	322	*235*	*227*	221	350	906	460	377	425	267		247
Pb	9	11		19	14	17	14	16	22	42	19		11							
Y	42	78	52	27 0	295	24 0	263	271	301	228	129	144	183	199	140	111	85	136		112
La	29	59	34	16 3	164	15 4	157	190	255	191	80	102	122	91	110	97	52		208	63
Ce	70	133	77	46 2	412	41 5	412	451	592	424	175	254	288	275	284	244	146	343		156
Pr	4.9	21							87	61	27		43						121	
Nd	45	96	57		296	22 7			361	263	122	161	189		187	154	125	176	19	
Sm	10	20	12	55	58	51	50	53	75	51	28	39	42	43	40	31	28	33	9	24
Eu	3.3	7.5	5.7	7.1	6.0	6.3	6.7	6.8	7.0	6.7	4.5	7.2	7.1	5.1	3.3	3.4	3.4	6.0	17	4.5

ACCEPTED MANUSCRIPT

Gd	12	22							61	51	27		39		39	28	30	28		
Tb	1.5	2.6	1.7	7.1	7.5	6.5	6.2	7.1	9.7	7.4	4.2	5.3	5.4	5.9					14	3.9
Dy	5.0	14							57	39	24		34		28	22	20	25		
Ho	1.2	2.7							12	8	5		7						7.4	
Er	2.9	6.4							31	21	13		17		13	11	9.2	13		
Tm	0.46	0.83							3.9	2.7	1.7		2.3						6.4	
Yb	3.1	4.5	4.0	20	16	18	15	23	24	17	11	13	15	16	12	10	7.5	13		12
Lu	0.50	0.64	0.61		2.3				3.6	2.5	1.8	2.1	2.1		0.34	1.7	1.6			1.8
[La/Yb] n	6.7	9.4	6.0	6.0	7.2	6.1	7.4	6.1	7.5	8.1	5.1	5.6	6.0	4.2	5.8	6.1	4.5	0.0	1.4	
Eu/Eu*	1.06	1.20	1.49	0.4 0	0.32	0.3 9	0.42	0.40	0.29	0.40	0.49	0.58	0.54	0.37	0.26	0.36	0.35	0.60	1.5	0.56
Peral (mol%)	0.73	0.63	0.88	0.6 7	0.75	0.6 9	0.71	0.74	0.80	0.83	0.77	0.72	0.71	0.69	0.49	0.62	0.41	0.80	0.75	0.75
Agp (mol%)	0.51	0.60	0.79	0.5 1	0.47	0.5 1	0.50	0.47	0.63	0.69	0.89	0.64	0.65	0.29	0.48	0.51	0.36	0.77	0.79	0.79
T sat zirc (°C)	865	943	1094	11 81	115 1	11 70	116 9	119 7	1158	1166	1111	1117	1106	1307	111 0	113 9	1180	115 8	1189	1133
T sat apat (°C)	946	1085	1050	93 7	948	91 3	925	945	965	966	978	984	989	1002	919	923	780	856	846	935

Origin of analyses: 78-32 and 84-2 from Wilmart et al. (1989); T-*: from Wilmart (1988); 93BN*: from Bolle (1998); Primitive jotunite: average of 8 analyses of chill samples: 70-20; 72-34; C6; C1; 80-12-3a; 80-12-4; 80-12-1 and 91-14-1; Evolved jotunite: average of 8 chill samples: 72-52, T2, 89-115, 75-20-2F, 89-26, 73-55, 78-21-1 and T22-1 from Vander Auwera et al. (1998b); 75-54-2: from Duchesne et al. (1989); 76-27 : this work; BM-* and PM-618: from Mitchell et al (1996); PM436 and MPK60a: from Scoates & Chamberlain (2003); AA-41: from Seifert et al. (2010). (a) SCc: Strong Creek complex; (b) PMa: Poe Mountain anortosite; (c) RMP: Red Mountain Pluton.

T sat zirc: temperature of saturation of zircon from Watson & Harrison (1983); T sat apat: apatite saturation temperature from Harrison & Watson (1984).

ACCEPTED MANUSCRIPT

Table 2 Major (wt.%) and trace element (ppm) compositions of ores from the Kydlandsvatn and Hestnes deposits

	Kydlandsvatn									Hestnes									
	00-14M	00-15	00-16	00-20	79-19-1B	00-17	66-182	00-14G	79-17-1	00-41	00-42	00-43	00-44	66-34	00-52'	00-58M	00-47	00-58	00-59G
SiO_2	0.01	1.49	0.17	1.39	1.04	0.10	0.13	0.01	0.86	6.33	0.30	0.72	0.79	1.07	0.59	0.26	2.12	0.89	0.48
TiO_2	32.7	29.8 8	34.6	28.5 0	28.30	44.10	43.90	42.20	45.60	13.1 1	11.5 3	12.0 5	11.5 4	11.48	16.20	19.00	21.4 0	22.7 0	24.10
Al_2O_3	2.02	2.49	2.03	2.64	2.51	0.91	0.85	1.35	0.80	2.58	1.52	1.61	1.54	1.59	2.32	2.19	3.04	2.60	2.51
FeO	27.7	25.2 6	28.2	23.7 0	26.10	34.50	34.30	33.00	35.70	23.3 9	21.2 6	20.3 6	20.5 8	18.97	27.30	31.50	37.7 0	37.5 0	35.50
Fe_2O_3	24.8	22.4 1	25.1	21.1 0	23.20	16.70	15.90	20.00	13.10	23.7 0	20.7 3	19.8 4	19.5 4	18.44	31.30	28.40	30.9 0	31.1 0	29.80
MnO	0.22	0.23	0.21	0.25	0.23	0.22	0.24	0.25	0.28	0.40	0.46	0.46	0.45	0.45	0.36	0.37	0.35	0.34	0.38
MgO	2.93	2.80	3.05	2.85	2.86	3.48	3.51	3.41	3.66	1.22	0.62	0.64	0.68	0.61	0.79	0.78	0.74	0.78	0.99
CaO	4.69	8.45	3.18	10.0 5	8.31	0.08	0.10	0.13	0.17	15.9 9	24.5 3	23.7 1	24.1 4	26.46	11.43	9.55	1.64	1.74	2.72
Na_2O	0.04	0.19	0.09	0.15	0.20	0.03	0.18	0.05	0.08	0.36	0.20	0.28	0.20	0.51	0.28	0.14	0.15	0.09	0.22
K_2O	0.01	0.01	0.01	0.01	0.01	0.01	0.04	0.01	0.01	0.06	0.01	0.02	0.02	0.02	0.01	0.01	0.04	0.04	0.01
P_2O_5	4.11	6.26	2.46	8.53	6.53	0.03	0.03	0.07	0.02	12.0 5	18.6 7	19.9 4	20.2 2	20.40	8.43	6.80	0.91	1.15	1.75
Total	99.23	99.4 7	99.1 0	99.1 7	99.29	100.1 6	99.18	100.4 8	100.28	99.1 9	99.8 2	99.6 3	99.7 1	100.0 0	99.01	99.01	98.9 9	98.9 3	98.45
Rb	0.11	0.33	0.16	0.19	0.13	0.48	0.57	0.32	0.48	0.85	0.44	0.41	1.35	0.52	0.31	0.29	0.8	0.84	0.73
Sr	69	111	49	151	123	12	14	13	25	138	176	181	175	190	93	81	26	17	32
Ba	23	5	23	25	24	26	27	24	27	53	33	21	23	46	30	14	34	16	30
V	3283	2521	2712	2192	2596	2710	2548	2662	2145	851	794	915	942	764	1412	1184	1599	2473	1506
Cr	273	301	194	187	236	234	261	156	132	81	90	177	129	239	315	433	1186	1371	567
Co	57	55	50	54	58	70	81	97	74	38	34	36	35	33	26	92	45	34	46
Ni	344	391	377	399	450	376	320	303	492	188	209	206	215	200	184	191	454	289	199
Cu	110	67	120	144	175	103	97	97	194	70	109	32	39	117	102	115	428	181	129
Zn	529	371	384	398	480	256	212	317	211	614	629	599	639	585	1142	1149	1406	1426	1345
Ga	42.4	28.8	38.6	36	37	24	17	29	18	36	34	28	30	31	59	61	62	65	73
Zr	212	207	179	198	181	225	195	206	255	631	214	394	480	661	1112	84	302	760	771
Hf	6.0	5.9	6.1	5.6	5.3	6.4	5.5	6.3	7.8	13.2	6.0	8.9	10.7	14.9	22.8	4.1	7.4	17.9	18.4
Zr/Hf	35	35	29	35	34	35	36	33	33	48	36	44	45	44	49	21	41	43	42

ACCEPTED MANUSCRIPT

Nb	34	30	30	33	30	36	34	44	47	48	47	43	44	53	49	54	64	63	81
Ta	1.8	1.6	2.4	1.5	1.5	2.4	2.0	3.0	2.3	0.9	1.7	1.1	1.2	1.6	1.3	1.6	2.0	1.4	3.1
Nb/Ta	19	18	13	22	20	15	17	15	20	55	28	39	38	32	38	34	33	46	26
U	0.3	0.32	0.26	0.37	0.37	0.25	0.26	0.23	0.23	1.4	2.4	1.9	2.1	2.4	1.3	1.2	0.38	0.39	0.54
Th	0.39	0.16	0.2	0.39	0.33	0.27	0.22	0.16	0.19	1.8	3.8	3.4	3.2	4.4	1.4	1.4	0.42	0.52	0.57
Th/U	1.3	0.5	0.8	1.1	0.9	1.1	0.8	0.7	0.8	1.3	1.6	1.7	1.5	1.8	1.1	1.1	1.1	1.3	1.1
Pb	1.1	2.0	0.93	1.3	1.3	0.96	1.2	1.4	3.4	4.2	3.3	4.3	4.4	2.9	2.6	1.3	2.5	1.9	3.1
Y	60	66	38	110	88	10	8	7	6	544	803	870	795	843	334	289	40	55	83
La	20	30	11	42	29	1.5	1.1	1.5	1.3	295	443	447	461	473	167	133	31	32	39
Ce	53	83	32	115	84	1.0	0.8	1.1	0.5	784	1207	1192	1226	1274	453	365	74	76	102
Pr	8.7	13	5.5	20	15	0.1	0.1	0.2	0.1	117	189	175	183	200	70	56	11	11	17
Nd	48	72	28	103	77	0.5	0.6	1.1	0.5	567	913	884	949	975	336	277	51	54	80
Sm	12	17	7.8	25	19	0.15	0.14	0.23	0.04	130	218	204	206	230	77	65	11	11	19
Eu	2.6	4.0	1.7	5.5	4.2	0.09	0.02	0.11	0.1	14	23	22	22	24	8.7	7.3	1.4	1.4	2.2
Gd	12	18	8.1	25	19	0.18	0.17	0.2	0.04	127	198	192	201	213	74	61	10	11	17
Tb	1.72	2.29	1.17	3.41	2.7	0.03	0.03	0.04	0.01	18	29	27	28	31	11	9.3	1.4	1.5	2.6
Dy	7.89	11	5.27	16	13	0.18	0.2	0.14	0.06	91	140	136	142	152	57	47	7.0	8.0	13
Ho	1.6	2.1	1.0	3.0	2.5	0.04	0.55	0.02	0.02	17	28	26	28	30	12	9.7	1.4	1.7	2.7
Er	3.2	4.3	2.1	6.2	5.0	0.11	0.17	0.05	0.05	38	58	58	60	64	25	21	2.9	3.7	5.7
Tm	0.4	0.48	0.26	0.68	0.51	0.02	0.03	0.01	0.01	4.5	6.8	6.5	6.8	7.3	3.0	2.6	0.39	0.45	0.68
Yb	2.4	2.6	1.5	3.7	2.9	0.13	0.25	0.04	0.1	24	36	36	37	40	17	14	2.0	3.0	4.0
Lu	0.29	0.31	0.18	0.46	0.37	0.02	0.04	0.01	0.03	2.92	4.3	4.3	4.48	4.66	1.96	1.75	0.31	0.42	0.51
(La/Yb)N	5.5	7.4	5.1	7.3	6.5	7.4	2.8	22.1	8.5	7.9	7.9	8.0	8.0	7.6	6.5	6.0	8.7	6.8	6.3
Eu/Eu*	0.67	0.70	0.66	0.68	0.67	1.68	0.40	1.57	7.65	0.34	0.33	0.34	0.33	0.33	0.35	0.35	0.41	0.39	0.37

ACCEPTED MANUSCRIPT

Table 3 Composition of Fe-Ti oxides in selected samples of Kydlandsvatn and Hestnes deposits

	Kydlandsvatn			Hestnes					
	Ilm 79-17-1	Ilm 00-15	Mgt 00-15	Ilm 00-41	Mgt 00-41	Ilm 00-47	Mgt 00-47	Ilm 66-33a	Mgt 66-33a
FeO	33.01	32.45	29.90	41.24	35.40	40.34	35.60	42.70	36.20
MnO	0.27	0.28	0.01	0.61	0.13	0.75	0.14	0.62	0.13
MgO	3.80	3.40	1.38	0.80	0.51	1.20	0.43	1.10	0.40
CaO	0.00	0.10	0.07	0.20	0.52	0.00	0.05	0.12	0.14
ZnO	0.010	0.005	0.085	0.014	0.164	0.007	0.270	0.012	0.260
Fe_2O_3	16.20	17.71	60.90	4.71	47.60	5.79	50.60	5.00	49.80
Al_2O_3	0.00	0.00	3.72	0.00	4.75	0.00	3.74	0.10	3.20
V_2O_3	0.322	0.363	0.872	0.022	0.270	0.032	0.352	0.020	0.340
Cr_2O_3	0.015	<	0.190	<	0.026	0.003	0.269	<	0.019
TiO_2	47.25	45.78	1.83	52.34	9.92	52.05	8.65	50.30	7.00
SiO_2	0.10	0.24	0.55	0.24	0.76	0.10	0.75	0.02	0.38
Total	100.98	100.33	99.51	100.17	100.06	100.27	100.85	99.99	97.87
Co (ppm)	100	<	110	<	40	<	80	50	NA
Ni (ppm)	120	70	450	30	30	20	130	0	80
Nb (ppm)	46	42	16	227	20	189	17	216	<
Zr (ppm)	93	135	54	298	<	153	9	217	<
Hem/Usp	0.146	0.163	0.057	0.005	0.314	0.018	0.266	0.051	0.218
Ilm/Mgt	0.854	0.837	0.943	0.995	0.686	0.982	0.734	0.949	0.782
XHem/NTi	0.125	0.141	0.052	0.005	0.279	0.017	0.243	0.048	0.203
XGk/NMg	0.140	0.126	0.072	0.030	0.026	0.045	0.022	0.041	0.022
Xpy/NMn	0.006	0.006	0.000	0.013	0.005	0.016	0.004	0.013	0.004
Temp (°C)		619			400		530		646
DFMQ (log unit)		3.1			-6.3		-3.3		-0.6

[a]analyses from Duchesne (1999) except for Zr and Nb concentrations
FeO calculated by charge balance
T°C and DFMQ(difference to FMQ buffer) calculated by use of QUILF (Andersen et al. 1993)
Detection limit (<): Cr= 9 ppm; Co= 10 ppm; Ni= 10 ppm; Zr= 5 ppm; Nb= 5 ppm; NA: not analysed

ACCEPTED MANUSCRIPT

Table 4 REE compositions (ppm) in apatite from the Kydlandsvatn and Hestnes nelsonites

	Kydlandsvatn			Hestnes		
	00-15	79-19-1 (a)		00-41	00-47	66-33 (a)
La	192	194		735	820	951
Ce	559	551		2195	2340	2649
Pr	88	94		306	335	
Nd	507	487		1555	1630	2108
Sm	110	123		354	379	466
Eu	27	26.8		41	39	44.5
Gd	109	131		346	360	423
Tb	14	16.7		49	50	67.9
Dy	69	85		253	258	300
Ho	12	12.6		46	43	55.1
Er	28	33.2		107	105	142
Tm	3	1.58		13	12	
Yb	15	17.2		64	62	83.9
Lu	2	2.2		8	8	10.4

(a) from Duchesne (1999)

ACCEPTED MANUSCRIPT

ACCEPTED MANUSCRIPT

Table 5 Rb-Sr and Sm-Nd isotopic compositions of apatites from Rogaland Fe-Ti deposits

Deposit	**Apatite**	**Rb ppm**	**Sr ppm**	**$^{87}Rb/^{86}Sr$**	**$^{87}Sr/^{86}Sr$**	**± 2σ**	**$(^{87}Sr/^{86}Sr)_i$ 930 Ma**	**Sm ppm**	**Nd ppm**	**$^{147}Sm/^{144}Nd$**	**$^{143}Nd/^{144}Nd$**	**± 2σ**	**$\varepsilon_{Nd@930}$**
Kydlandsvatn	79-19-1	<	541	-	0.706233	0.000010	**0.706233**	123	487	0.1527	0.512343	0.000014	**-0.53**
Kydlandsvatn	90I	<	484	-	0.706241	0.000008	**0.706241**	149	497	0.1813	0.512364	0.000007	**-3.52**
Kydlandsvatn	90J	<	594	-	0.707476	0.000010	**0.707476**	116	400	0.1754	0.512552	0.000009	**0.86**
Kaknuden	66-11	<	504	-	0.706389	0.000008	**0.706389**	138	608	0.1373	0.512355	0.000014	**1.56**
Kaknuden	66-163	<	518	-	0.706214	0.000010	**0.706214**	139	538	0.1563	0.512359	0.000007	**-0.63**
Rødemyr II	66-15	<	500	-	0.706450	0.000011	**0.706450**	158	609	0.1569	0.512352	0.000010	**-0.85**
Hestnes	92-23D	<	396	-	0.708270	0.000010	**0.708270**	439	1994	0.1331	0.512272	0.000011	**0.42**
Hestnes	66-33	<	400	-	0.708411	0.000009	**0.708411**	466	2108	0.1337	0.512309	0.000013	**1.08**
Hestnes	66-150	1.05	385	0.0079	0.709540	0.000009	**0.709435**	395	1737	0.1375	0.512298	0.000010	**0.41**

ACCEPTED MANUSCRIPT

ACCEPTED MANUSCRIPT

Table 6 Comparison of the chilled jotunite #78-32-3 with the range of compositions of its conjugate immiscible melt (quartz mangerite #78-32) calculated with the melt-melt partition coefficients for Si, Ti, Fe, Ca, K and P from Bogaerts & Schmidt (2006)

Element	D (L^M/L^F)	Qtz Mangerite 78.32([a]) wt%	Qtz Mangerite Experimental Fe-liq. wt%	Chill 78-32-3([a]) wt%
SiO_2	0.66± 0.12	65.71	35.5-51.2	50.58
TiO_2	3± 1	0.99	2.0-4.0	3.89
FeO_t	3.2± 0.4	7.53	21.1-27.1	24.67
CaO	2.8± 0.6	2.56	5.6-8.7	5.7
K_2O	0.26± 0.16	5.04	0.51-2.14	1.44
P_2O_5	7.5± 5.0	0.51	0.9-6.4	1.26

([a]) from Table 1

ACCEPTED MANUSCRIPT

ACCEPTED MANUSCRIPT

Graphical abstract

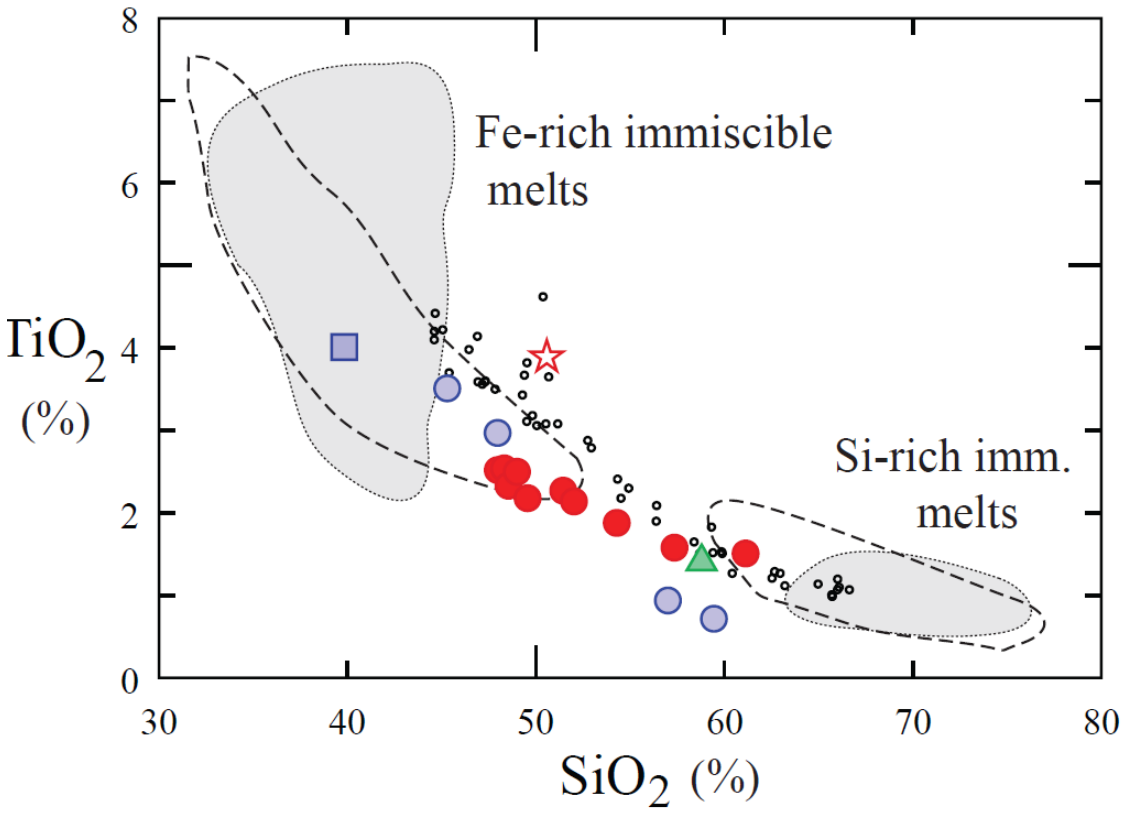

ACCEPT

ACCEPTED MANUSCRIPT

Highlights

- Two nelsonites deposits with contrasted mineral compositions in Rogaland
- One is a cumulate in a ferrodiorite/jotunite magma
- The other, rich in REE, Zr and Cr, possibly crystallised from Zr-rich jotunite
- Some Zr-rich jotunites are immiscible melts with quartz mangerite magmas

ACCEPTED MANUSCRIPT